Embedded regional/Local-scale model of natural transients in saline groundwater flow Illustrated using the Beberg Site

Niko Marsic
Kemakta Konsult AB

Lee Hartley, Paula Sanchez-Friera
Serco Assurance, UK

Arnfinn Morvik
BSSI, Norway

April 2002

SKB

Embedded regional/Local-scale model of natural transients in saline groundwater flow Illustrated using the Beberg Site

Niko Marsic
Kemakta Konsult AB

Lee Hartley, Paula Sanchez-Friera
Serco Assurance, UK

Arnfinn Morvik
BSSI, Norway

April 2002

Summary

The main focus of this report is to develop and test a methodology for performing large simulations of transient variable density flow. Several developments were made to NAMMU to enable such calculations. The following lists the findings of this study:

1) **Feasibility:** it is numerically feasible to construct large (0.5 million elements) embedded models of transient variable density flow with a relatively fine mesh (about 35m) of the site-scale.

2) **Stochastic simulation:** performing stochastic realisations of long transients is just possible, although the requirements on CPU and disk to store the results for 100 realisations, say, would be significant. As an indication, about 19 realisations of the current model could be run on a Sun Enterprise 450 ($4 \times$ UltraSPARC-II 400MHz) computer in one week if all four processors are fully utilised.

3) **Embedded grid:** the nesting of a refined site-scale model (35m elements) within a coarser (100m) regional-scale mesh for variable density flow was tested successfully. It was found that grading the refinement around the site-scale to avoid a large step change in element size was beneficial for convergence and stability. This may be less of an issue if a more sophisticated preconditioner was used.

4) **Solver:** the most efficient and stable scheme was obtained by decoupling the flow and transport equation at each time-step. GMRES (Generalised Minimum Residual) was the most robust conjugate gradient method for this problem.

5) **Boundary conditions:** a set of relatively complex non-linear boundary conditions had to be applied for both pressure and salinity on the top and vertical boundaries to give the system sufficient freedom to approximate realistic conditions over a large area and long times. It was important that both flow and a flux of salinity could cross each boundary, and that the direction and magnitude could evolve in time.

6) **Calibration on salinity:** model predictions of the salinity in the deep boreholes were used to calibrate the model parameters and structural representation. As for the SR 97 regional-scale model the high salinity below Zone 2 could not be reproduced with a highly transmissive zone. A reasonable match could only be achieved if a semi-impermeable band be included in the core of Zone 2, and the position of Zone 2 had to be taken from the detailed geometry defined in Andersson *et al.* (1991) rather than SR 97.

7) **Structural model**: the calibration demonstrated the important effect that sub-horizontal fracture zones could have on deep groundwater flows, and the importance of having a good structural interpretation of such zones. Aspects such as hydraulic anisotropy, layering, fracture zone truncation and interconnection will be important to characterise in any site either by direct measurement and/or by using modelling to test the ability of different structural models to predict hydraulic and chemical properties in deep boreholes. In fact, this is a good example of how a flow model calibration exercise can augment structural interpretation and help constrain it.

8) **Flexible representation:** new tools for representing fracture zones and rock volumes allow flexibility in how a structural model is represented e.g. wedge shaped zones and hydraulic anisotropy.

9) **Modelling barriers:** proved to be non-trivial since approximating the thickness or representation of flow through a thin barrier relative to the grid size can lead to an over-prediction of flow rates through barriers. For standard elements, if only a thin band of elements, one or two thick, is used to model a semi-impermeable barrier, then the flow across the zone may be larger than expected. This is because small flows can 'leak' across element corners because of the lack of localised mass balance. This is not the case with mixed-elements, which motivates more investigation of this element type.

10) **Transport statistics:** indicate that neither salinity nor release-time has a great effect on statistics of travel times or canister flux. Salinity leads to slightly higher canister flux, but slightly longer travel times and around double the path lengths. Perhaps more important is the structural model for Zone 2. A low permeability core in Zone 2, as used in Case 3-5, leads to slightly longer median travel time, but also much less variance with fewer short paths compared to Case 1 which used the SR 97 representation of Zone 2. These conclusions are very site specific. The Beberg site is located about 15km inland, and hence conclusions on the importance of release time are likely to be different to those for a site nearer the coast.

11) **Comparison with previous studies:** many of the conclusions from the SR 97 regional model have been shown valid for this more detailed study. For example, the same parameters and structural model were needed to get a calibration on deep salinity profiles. Travel times and exit locations are broadly consistent, and the problem with particles exiting the SR 97 model out of the vertical side has been solved by extending the model northwards. The new model shows that the exit location for these paths is Skälsjön. Comparing with the site-scale models of SR 97 travel times are much longer here mainly because of not enhancing the permeability of the rock blocks, but also due to salinity and the structural model for Zone 2. Results are most similar to the SR-97 regional model.

Sammanfattning

Det huvudsakliga målet med den här rapporten är att utveckla och testa en metodik för att genomföra stora transienta simuleringar av flöde med variabel densitet. Flera modifieringar av NAMMU utfördes för att möjliggöra sådana beräkningar. Nedan följer en lista på slutsatser från arbetet:

1. **Genomförbarhet**: det är numeriskt möjligt att generera stora (0.5 milj. element) sammanlänkade transienta modeller med flöde med variabel densitet med ett relativt fint diskretiserat nät (ca 35m) på lokal skala.

2. **Stokastisk simulering**: att genomföra stokastisk simulering med stora tidsspann är i princip möjligt även om kraven på CPU och diskutrymme för att lagra resultaten för tex 100 realiseringar blir stora. Som jämförelse kan nämnas att det skulle ta ca 1 vecka att genomföra 19 realiseringar med den aktuella modellen på en Sun Enterprise 450 ($4 \times$ UltraSPARC-II 400MHz) med fyra processorer fullt utnyttjade.

3. **Sammanlänkade nät**: en fint diskretiserad modell på lokal skala (35m element) nästlad inuti en grövre (100m) modell på regional skala testades med framgång för flöde med variabel densitet. Det visade sig att en gradvis ökning av element-storleken utåt från lokalmodellen, i syfte att minska förändringen i storlek hos elementen, förbättrade konvergensen och stabiliteten hos modellen. Detta problem kan möjligen minskas med en bättre prekonditionerare och numerisk lösare.

4. **Numerisk lösare**: det mest effektiva och stabila tillvägagångssättet var att lösa flödesekvationen och transportekvationen separat (icke kopplat) vid varje tidssteg. GMRES (Generalised Minimum Residual) var den mest robusta metoden för det aktuella problemet.

5. **Randvillkor**: en uppsättning relativt komplexa icke-linjära randvillkor användes för tryck och salthalt på topp- och sidoränderna i syfte att ge systemet tillräcklig frihet att beskriva realistiska förhållanden över en stor yta och under lång tid. Det var viktigt att låta både saltflöde och -flux att passera alla ränder samt att riktning och storlek kunde variera med tiden.

6. **Kalibrering m a p salthalt**: beräknade salthalter i de djupa borrhålen användes för att kalibrera modellparametrarna och strukturmodellen. De höga salthalterna som erhölls under Zon 2 i regionalmodellen för SR 97 kunde inte återskapas med en högtransmissiv zon. En hyfsad överensstämmelse kunde endast uppnås genom att använda sig av ett semi-impermeabelt lager i mitten av Zon 2 samtidigt som läget och utseendet ändrades enligt Andersson *et al.* (1991) istället för som i SR 97.

7. **Strukturmodell**: kalibreringen visade på betydelsen av subhorisontella sprickzoner för grundvattenflöde djupt ned i berget och vikten av att ha en god strukturtolkning av sådana zoner. Aspekter som hydraulisk konduktivitet, skiktning, trunkering av sprickzoner och kontakt mellan sprickor blir viktiga parametrar att karakterisera för alla platser antingen genom direkt mätning och/eller genom användning av modellering för att testa förmågan hos olika strukturmodeller att prediktera

hydrauliska och kemiska förhållanden i djupa borrhål. Faktum är att detta är ett bra exempel på hur en kalibreringsövning av en flödesmodell kan styrka den strukturella tolkningen.

8. **Flexibel representation**: nya verktyg för representation av sprickzoner och bergvolymer förbättrar möjligheterna att representera mer avancerade strukturer, så som icke-planparallella volymer och hydraulisk anisotropi.

9. **Modellering av barriärer**: visade sig vara icke-trivialt då approximation av tjocklek eller representation av flöde genom en tunn barriär jämfört med elementstorleken kan leda till en överskattning av flödet genom barriärer. Om man endast använder sig av ett eller två standardelement i tjocklek för att modellera en semi-impermeabel barriär kan flödet tvärs zonen bli större än väntat. Detta beror på att små flöden kan "läcka" över elementhörnen på grund av avsaknaden av lokal massbalans. Detta är inte fallet med "mixed"-element vilket motiverar mer undersökning av dessa elementtyper.

10. **Transportstatistik**: indikerar att varken salthalt eller tidpunkt för start av partiklar har stor effekt på statistiken för gångtider eller flöden. Saltet leder till något högre flöden i förvarsområdet men också något längre gångtider och ungefär dubbelt så långa flödeslinjer. Viktigare är då möjligen strukturmodellen för Zon 2. En lågpermeabel kärna i Zon 2, vilket användes i Case 3-5 leder till något större median för gångtiden men också lägre varians med färre korta partikelbanor, jämfört med Case 1 (samma representation av Zon 2 som användes i SR 97). Dessa slutsatser är dock väldigt platsspecifika. Beberg befinner sig 15 km från kusten. Således kan man förvänta sig att slutsatserna för betydelsen av val av tidpunkt för start av partiklar kommer att skilja sig för en plats närmare kusten.

11. **Jämförelse med tidigare studier**: många av slutsatserna från regionalmodellen i SR 97 har visat gälla även den här mer detaljerade modellen. Till exempel behövdes samma parametrar och strukturmodell för att erhålla en modell kalibrerad med avseende på salthalten i de djupa borrhålen. Gångtider och utsläppsplatser är i stort överensstämmande och tidigare problem med partiklar som nått sidoränderna hos modellen har lösts genom att utvidga modellen norrut. Den nya modellen visar att utsläppsplatsen för dessa partiklar är Skälsjön. Jämfört med modellerna för lokal skala i SR 97 är gångtiderna här mycket längre. Detta beror i huvudsak på att permeabiliteten för bergmassan runt förvarsområdet inte höjts men även på saltet och strukturmodellen för Zon 2. Resultaten stämmer bäst överens med regionalmodellen i SR 97.

Contents

1   Background and Objectives

This report describes the development of a nested approach to the simulation of the effects of marine transgressions and post-glacial rebound on salt transport and groundwater flow at sites in proximity to the coast. For illustration, a large three-dimensional model of the Beberg site is described and compared with previous models from SR 97 and other recent studies.

This is primarily a feasibility study for simulating transient flows with salinity from 4,000 years BP through the present day and 5,000 years into the future. Issues to be addressed include:

– Is it feasible to model salinity driven flow with an embedded grid?

– What numerical size of model is practicable for non-linear transient calculations?

– How should the position and prescription of boundary condition be chosen for such models?

– How feasible is stochastic continuum modelling of transient salt transport?

– How do the transport results compare with SR 97?

– How sensitive are the transport results to when particles are released either using a snapshot of the flow-field or the time-varying flow-field?

– What enhancements are needed to the Avizier for NAMMU software are necessary for visualising?

The finite-element software NAMMU for solving non-linear hydrogeological systems was used in this project. Developments of the software were necessary to implement complex boundary conditions that describe transient saline flow on the regional-scale, and to solve the non-linear coupled salt transport and groundwater flow equations efficiently for large three-dimensional meshes. Section 2 describes the development of the boundary conditions. Section 3 describes the development of the numerical solution scheme. An application of the developed approach to a new model of the Beberg site is described in Section 4. A calibration of the model against present day salinity measurements in deep boreholes and calculations of predicted transport statistics are include in Section 5 along with a comparison with SR 97 and previous studies. A summary is given in Section 6.

2   Governing equations and boundary conditions for transient saline flow

In NAMMU (Cliffe et al., 1998) the equations for transient groundwater flow with variable density are modelled in terms of the variables residual pressure, $p^R(x,t)$, and salt concentration (or mass -fraction), $c(x,t)$, and are described below.

Continuity:

$$\frac{\partial}{\partial t}(\phi\rho_l) + \nabla\cdot(\rho_l\mathbf{q}) = 0 \quad .$$

Darcy's law:

$$\mathbf{q} = -\frac{\mathbf{k}}{\mu}\left(\nabla p^R - [\rho_l - \rho_0]\mathbf{g}\right) \quad .$$

Salt transport:

$$\frac{\partial}{\partial t}(\phi\rho_l c) + \nabla\cdot(\rho_l\mathbf{q}c) = \nabla\cdot(\phi\rho_l\mathbf{D}\cdot\nabla c) \quad .$$

Here, $\phi(p^R)$ is the total porosity, $\rho_l(c,p^R)$ is the fluid density, ρ_0 is the freshwater density, $\mathbf{k}$ is the permeability tensor, μ is the fluid viscosity, $\mathbf{g}$ is the gravity vector, $\mathbf{D}(\mathbf{q})$ is the hydrodynamic dispersion tensor. The transient (first) term in the continuity equation can be expanded using the chain rule and reparameterised in terms of storage rather than compressibilities to give:

$$\frac{\partial}{\partial t}(\phi\rho_l) = \frac{S}{g}\frac{\partial p^R}{\partial t} + \phi\frac{\partial\rho_l}{\partial c}\frac{\partial c}{\partial t} \quad .$$

where S is the specific storage coefficient. The standard form for the fluid density is based on a mass-fraction dependence on the concentration:

$$\rho_l = \left(\frac{1-c}{\rho_0} + \frac{c}{\rho_s}\right)^{-1} \quad ,$$

where ρ_s is the saltwater density. Hence, the concentration, c, is a non-dimensional mass fraction that varies between 0 for freshwater of density ρ_0, and 1 for saltwater of density ρ_s. The hydrodynamic dispersion tensor is defined in terms of the local velocity using suffix notation as

$$\mathbf{D} = \frac{D_m}{\tau}\delta_{ij} + \alpha_T v\delta_{ij} + (\alpha_L - \alpha_T)\frac{v_i v_j}{v} \quad ,$$

where D_m is molecular diffusion of salt, τ is the tortuosity, α_L is the longitudinal dispersion and α_T is the transverse dispersion. The porewater velocity vector, v, is defined as

11

$$v = \frac{q}{\phi} \qquad \text{and} \qquad v = (v \cdot v)^{\frac{1}{2}} \quad .$$

Boundary conditions on these equations are posed as either Dirichlet conditions on p^R and c, or in terms of the mass flux F_p and the concentration flux Fc. The fluxes across a boundary surface with outward unit normal $\boldsymbol{n}$ are defined as

$$F_p = \rho_l q \cdot \boldsymbol{n} \quad ,$$

$$F_c = (\rho_l q c - \phi \rho_l \boldsymbol{D} \cdot \nabla c) \cdot \boldsymbol{n} \quad .$$

The default boundary conditions are $F_p = 0$, $F_c = 0$.

For Beberg boundary conditions for both pressure and salinity were required that represented marine transgressions and post-glacial rebound from 4,000 years ago (Hartley *et al.*, 1998), when the area was largely under the Litorina Sea, through the present situation and into the future.

Over such long periods of time there are no obvious 'natural' boundary positions for the vertical boundaries, such as water divides, that remain valid over the long transients considered. Therefore, the boundary conditions on the vertical sides need to be flexible to allow flow and salinity to cross the boundaries and evolve in time. The boundary condition on pressure/flow was hydrostatic:

$$q_z = 0 \Rightarrow \frac{\partial p^R(x,t)}{\partial z} + g(\rho(x,t) - \rho_0) = 0 \quad .$$

This allows flow to cross the boundaries vertically and evolve as the groundwater density changes as salinity is flushed out the system. This condition was applied on all vertical boundaries. The boundary condition is non-linear as it couples the boundary pressure to salinity that is a function of flow conditions. It is implemented in NAMMU by applying a finite-element equation at each node on the vertical boundary surfaces. This was a new development in NAMMU, and hence had to be tested. It was found that boundary condition gave consistent results for standard linear and quadratic elements using a direct solution method. However, the boundary condition cannot be used for quadratic elements with the current iterative solvers in NAMMU as the equations have an anti-symmetric form that is not positive definite. This could be remedied by using more sophisticated preconditioners, but for this reason linear elements were used throughout this study. The boundary condition for salinity on the vertical sides was also non-linear. At places (and times) where flow was outwards, then an outflow condition was applied. That is, an advective flux of salinity was taken out of the model

$$F_c = (\rho_l q c) \cdot \boldsymbol{n} \quad .$$

In places where flow was inward, the salinity was set to half the maximum value, $c=0.5$. For this prescription to evolve in time the boundary conditions needs to change as the concentration and flow change with time. For this reason it was implemented

12

numerically as a 'generalised flux' boundary condition in NAMMU with a penalty
function used to simulate the Dirichlet type condition on inflow boundaries

$$F_c = \frac{1}{\varepsilon}(\rho_l q[c - 0.5]) \cdot \boldsymbol{n} \quad ,$$

where ε is a constant chosen to define the penalty function. Here ε was set to 0.01.
This flux based boundary ensures c is always about 0.5 by injecting an appropriate flux
if $c<0.5$, and extracting a flux of salt if $c>0.5$. The reason for setting the boundary
condition in this way is that it can be defined simply by a common function for inflow
or outflow and the switch between boundary conditions between different places or
time-steps can be made automatically as the system evolves. These relatively complex
boundary conditions were found to be the only ones that gave an acceptable
representation of transient conditions on a regional-scale that was stable. Due to the
complexity of the model, heterogeneity arising from regional fracture zones and non-
linear coupled equations, as well as the regional-scale flows, all other boundary
conditions tried lead to numerical problems such as salt getting trapped around fracture
zones or corners and eventually 'blowing up'. The only other stable boundary
conditions that could have been used would have been constant Dirichlet values for
pressure and salinity, but this would not have been realistic as there is no obvious
steady-state situation or values for the site considered.

On the top surface a topographic head was used, but this evolved in time as a linear
function equivalent to a rise in topography of 7mm/year:

$$p(z,t) = \rho g * \max(z + 0.007 * t, 0)$$

Where $p(z,t)$ is the residual pressure at a current elevation of z and at time t between –
4000 years BP to 5,000 years AP. For land below the instantaneous sea-level, a head of
zero is used. This assumes a linear rate of land-rise. A more sophisticated function of
land-rise over long times could easily be used instead. The top-surface salinity boundary
condition was $c(\boldsymbol{x},t)=1$ below the instantaneous sea-level, $c(\boldsymbol{x},t)=0$ above sea-level
where there was recharge, and advective outflow condition for salinity where there was
discharge. Again, a non-linear generalised flux boundary condition with a penalty
function to simulate the Dirichlet part was used to implement this complex prescription.
It should be noted that regions of recharge and discharge evolved in time.

The bottom boundary was at –1500m where no flow and zero flux of salinity was
specified. The initial condition 4,000 years BP were calculated for $c(\boldsymbol{x},-4000)=1$, and
pressure was calculated from a steady-state calculation of the instantaneous flow at this
time. A groundwater density of 992 kg/m^3 was used for freshwater and 1025 kg/m^3 for
fully saline water. This is consistent with the regional-scale model of SR 97 (Hartley et
al., 1998).

3 Development of numerical solution scheme

The groundwater flow and salt transport equations in NAMMU are in their standard form fully coupled. That is, groundwater flow depends on variations in density, and in turn, salt transport depends on advective flow rates and hydrodynamic dispersion. This gives a set of non-linear equations that ordinarily are solved by a Newton-Raphson iteration scheme. The use of complex non-linear boundary conditions that couple flow and salinity introduces extra numerical complexity to the system that may have required many Newton-Raphson iterations per timestep. Given that it was desired to use models with high levels of refinement, about 500,000 finite-elements, then solving the fully-coupled equations would have lead to unacceptable run-times. Instead, a more efficient numerical scheme was implemented in NAMMU specific to transient salt transport. The basic approach is to decouple the solution of pressure and salt by linearising the equations. Hence, at each timestep a two-step procedure is used:

1) calculate the current pressure profile based on the salt profile from the previous timestep. This gives the new velocity and hydrodynamic dispersion fields.

2) calculate the current salt profile based on the new velocity and dispersion.

This is a simplification of the transient equations, but one that is a good approximation providing the timestep is chosen to be small relative to times appropriate to advective flow rates and the hydraulic diffusivity. It was also found that this scheme was generally preferable in terms of its stability. Solving the fully coupled salt transport equations often leads to many iterations largely because the form of classical model for dispersion is non-linear. The size of timesteps used were similar to those found appropriate in the SR97 regional model, except the earlier timestep sizes were halved here to give better accuracy on the more refined grid. Very small timesteps are used initially to resolve the fast transient of salt being flushed out of the onshore fracture zones. The timestep is gradually increased as salinity in the fracture zones reaches a quasi-equilibrium and the rock mass is slowly flushed of salt. The exact time-step values used are reported in Table 4-3. A total of about 100 timesteps were used to calculate a transient evolution from 4,000 years BP to 5,000 years AP. A fully implicit Crank-Nicholson transient scheme was used.

Another development to NAMMU that was required for this project was to extend IFZ (Implicit Fracture Zones) to calculate an effective porosity for each finite-element. This is because in SR97 it was found that to achieve a good match to salinity profiles in deep boreholes a different value for the total porosity had to be used for the fracture zones and rock mass. The values used were 5% for fracture zones, and 2% for the rock mass. It should be noted that these are total porosities representing slow diffusion processes, in which there is time for matrix diffusion into the total connected pore space, that are appropriate to long-term natural transients. These values are much higher than the standard value, 10^{-4}, used in the transport/pathline calculations where for reasons of conservatism it is assumed that solutes advect through channels without diffusion into the full matrix volume. The effective porosity for each block was calculated as

$$\phi_t = V_f \phi_f + (V - V_f)\phi_r$$

where ϕ_t is the total porosity, ϕ_f is the total fracture porosity, ϕ_r is the rock mass porosity, V is the block volume and V_f is the total fracture volume.

4 Application to the embedded regional/site-scale modelling of Beberg

4.1 Mesh and fracture zones

The application of transient salt transport at Beberg was reconsidered to demonstrate what is now possible in NAMMU compared to the regional-scale modelling performed for SR 97. Developments in the software since SR 97 used include: IFZ, embedded models, iterative solvers, and general performance improvements in addition to those described in Sections 2 and 3. The same concepts of hydrogeology and structural model were used. The main differences were that the model was extended to the coast in the north-east, the boundary in the west was slightly shortened, and extra regional-scale zones were included to the north. The extension of the boundary northwards (about 10km) was motivated by a need to address a criticism of the SR 97 in that for the saline case some paths exit the model through the vertical northern boundary. From that model it was not clear if these long paths were realistic, or just a consequence of the proximity to the boundary and the condition applied there.

Figure 4-1 shows the outline of the new model domain superimposed on a topography map. Potential receptors for long paths are the lake Skälsjön, a valley to the northeast than runs east-west or the coast itself. The NAMMU grid is set up using patches, which are larger high level blocks that are later discretised into finite elements. The patches, which are not used for calculations, can have varying discretisations in different directions and therefore offer more flexibility when generating the grid. The figure also shows the new regional-scale fracture zones that needed to be included to model the hydrogeology on the larger region. The overall model is about 20km (SW-NE) by 15km (SE-NW) or about 300 km^2. The western boundary was shortened slightly to run along a ridge. The area in green shows the approximate extent of the local-scale region.

Figure 4-2 shows the finite-element mesh together with all fracture zones. The fracture zones are coloured according to permeability with the new regional-scale zones being coloured yellow as they all have the same moderate value. The mesh size is about 100m in the regional-scale, although this increases toward 200m in the far north. The grey area in the middle is the position of the embedded local-scale model that has a much finer 35m element-size. In total, there are 484,040 linear cubic elements used and about 1,030,000 freedoms. This compares with 3,478 quadratic elements and 35,252 freedoms for SR 97. Hence, the new model represents a very significant increase in resolution and consequentially accuracy. Figure 4-3 shows the nesting of the embedded grid. A concentric ring of elements to grade the refinement between the local-scale and regional-scale was introduced as it improved the convergence of the iterative solver for salt transport. This graded refinement from about 105m down to 70m, so that at the constraint interface there are 2 (horizontal) by 3 (vertical) elements in the fine-mesh connecting to 1 element in the coarse mesh.

Figure 4-4 shows the regional- and local-scale fracture zones. Figure 4-5 shows a close-up of the local-scale fracture zones including the sub-horizontal Zone 2 that lies above

the position of most of the repository. The new regional-scale zones are shown in Figure 4-6 along with the finite-element mesh. A thickness of 100m and a permeability of $1.23 \ 10^{-12} \ m^2$ was used for these zones. Figure 4-7 is an alternative 3D view of the fracture zones. Figure 4-8 shows a close-up of the mesh on the local-scale and the corresponding fracture zones.
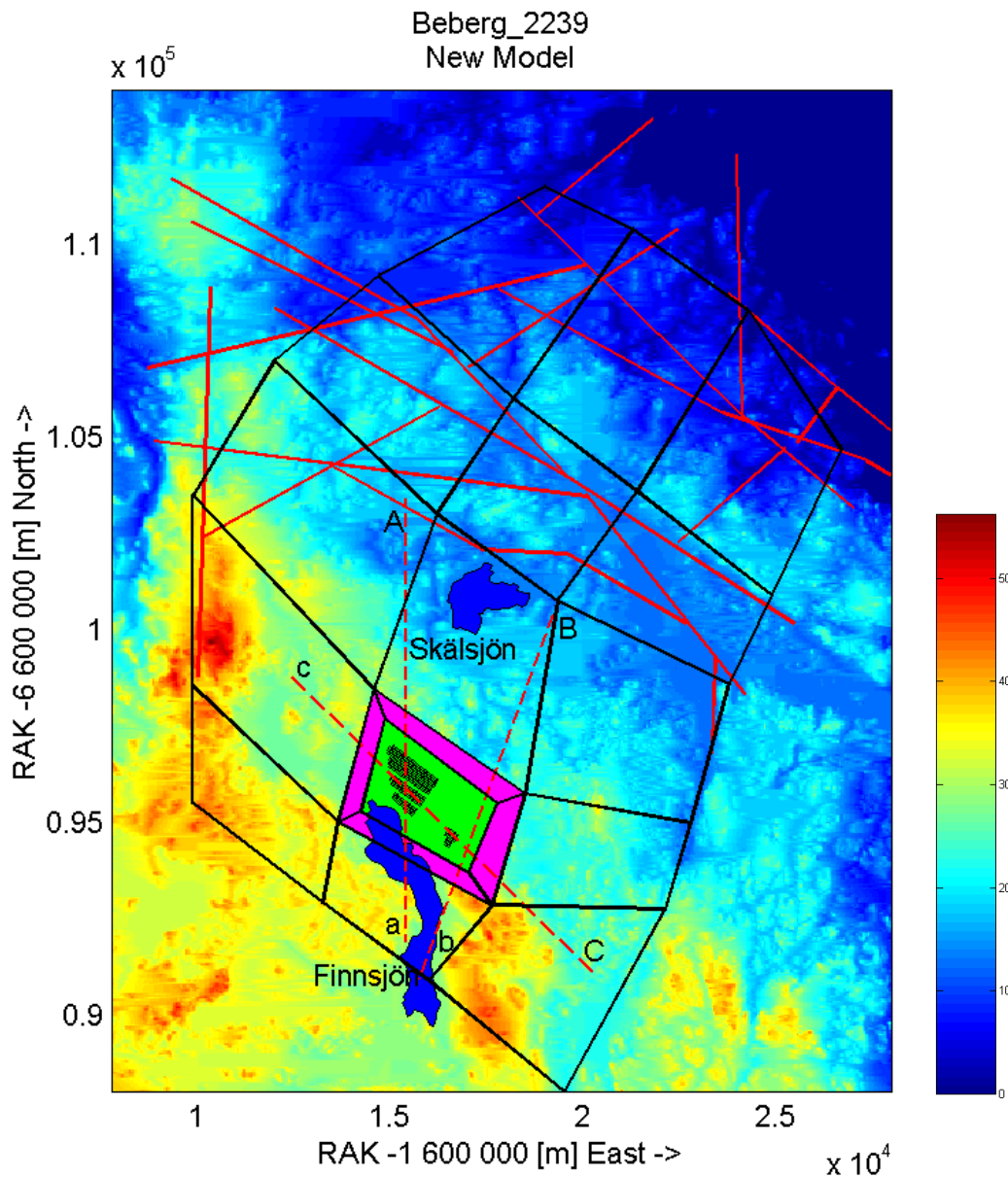
Figure 4-1　　*Plan view of current topography with positions of new regional-scale fracture zones (red) and the patch grid (see explanation above)(black) to show the model extent. The local-scale model (green) is surrounded by an intermediate region of graded refinement (pink). The positions of the three vertical slices a-A, b-B and c-C used in the calibration are indicated as dashed red lines.*
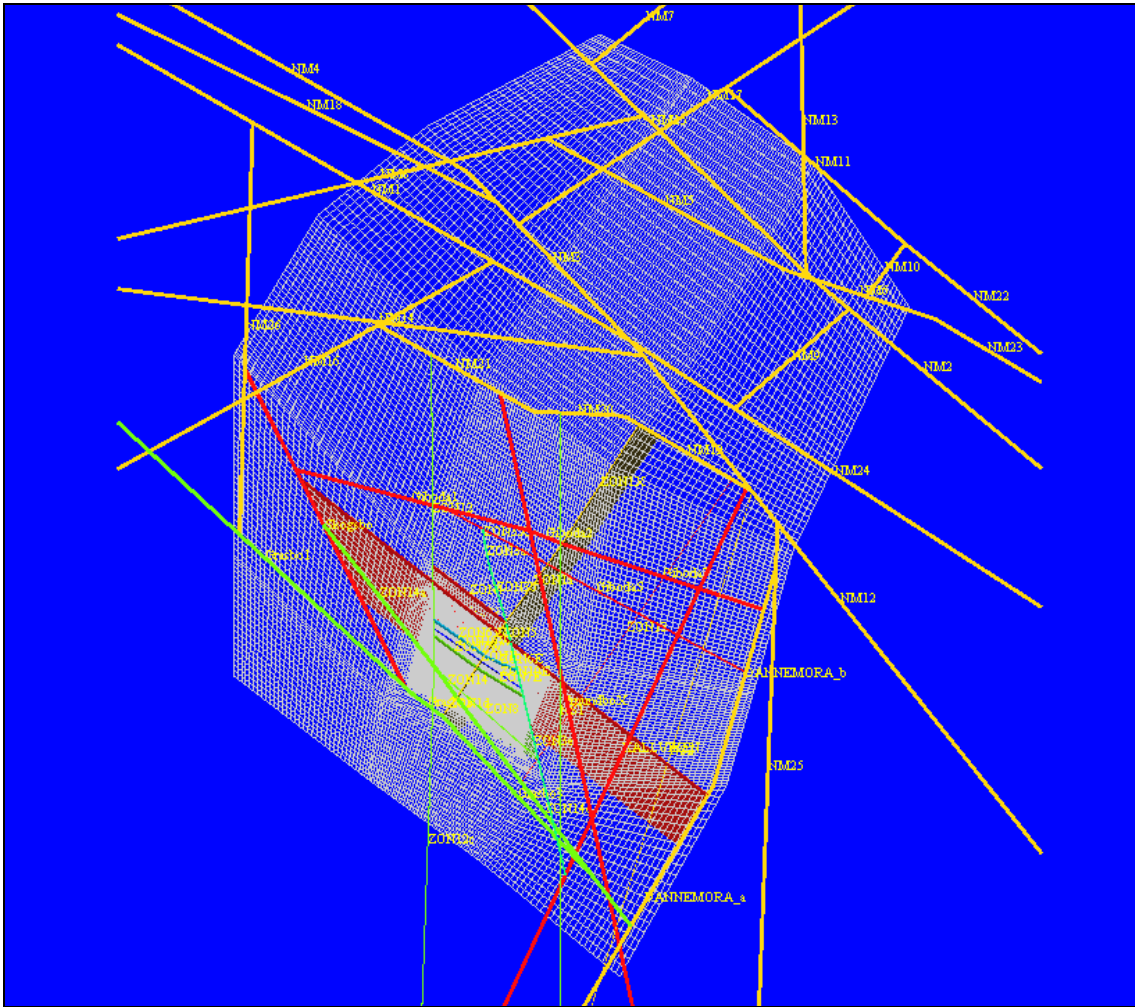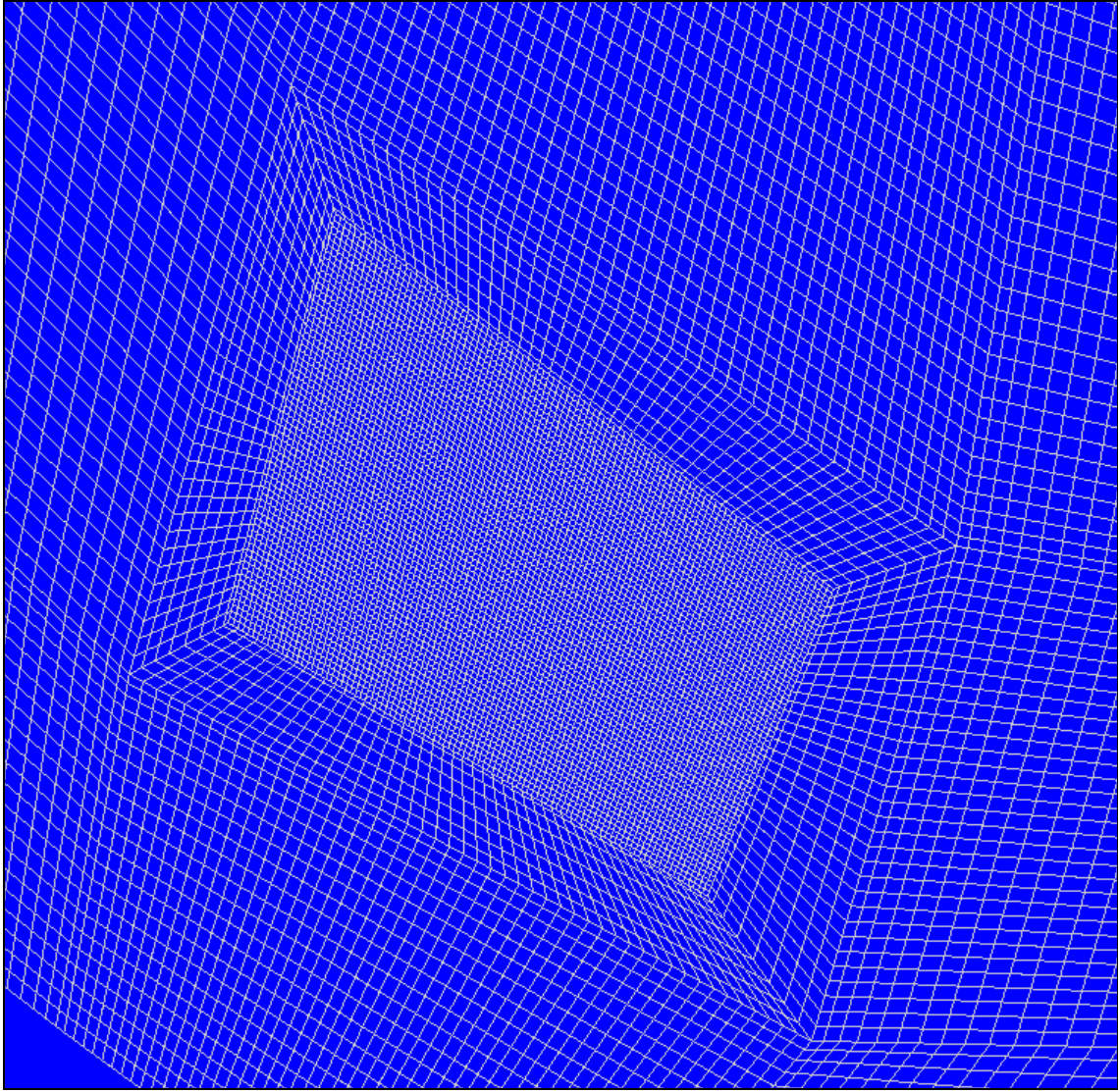
Figure 4-2 *Plan view of the new extended grid together with all fracture zones represented in the model. The fractures are coloured according to log10 permeability. Red showing higher values and blue lower.*

Figure 4-3   Plan view of the grid zoomed in on the site-scale. The site-scale region (in the centre) is refined to 35 m with concentric refinement around the region increasing to a mesh size of about 100 m. North is up the page.
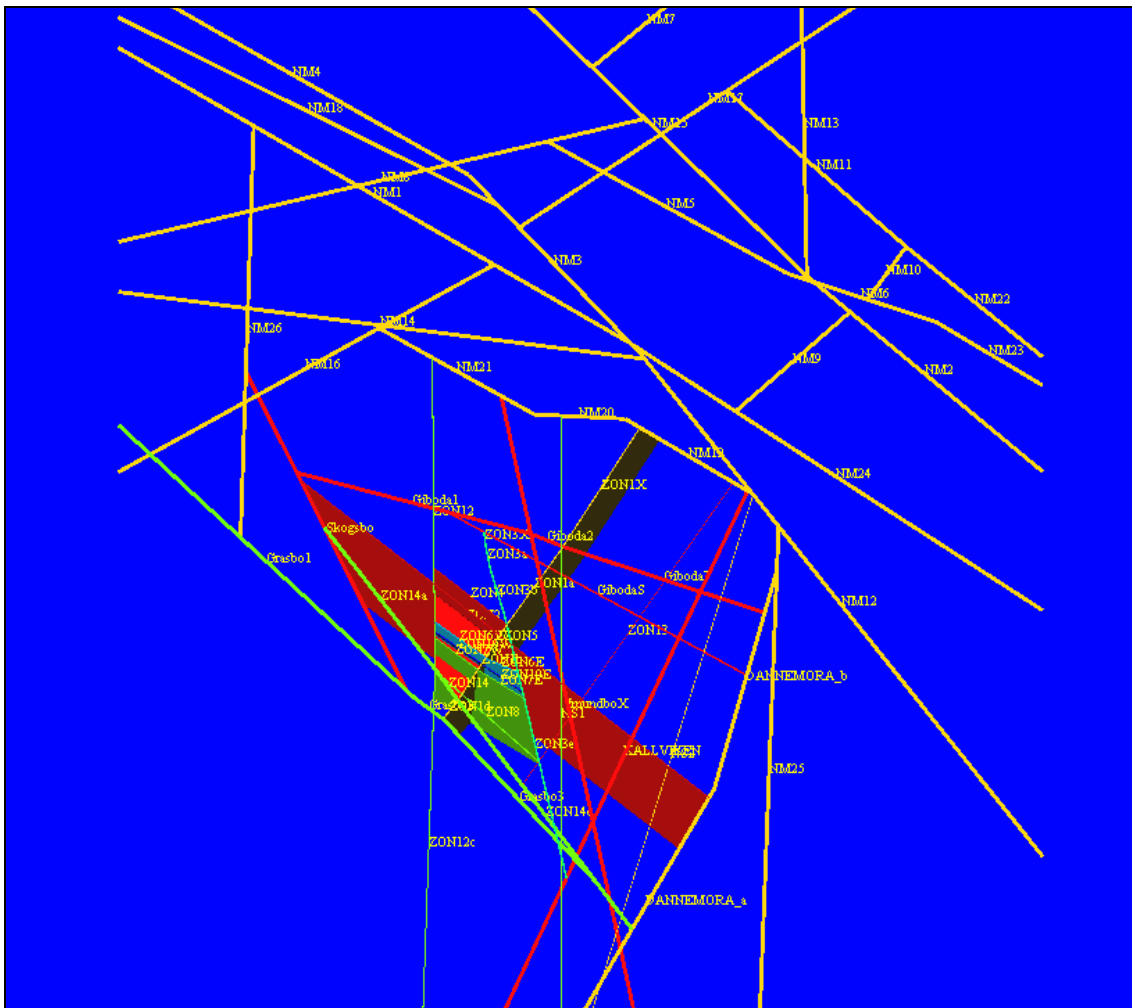
Figure 4-4   Plan view of all the fracture zones represented in the model. The fractures are coloured according to permeability. Red showing higher values and blue lower.
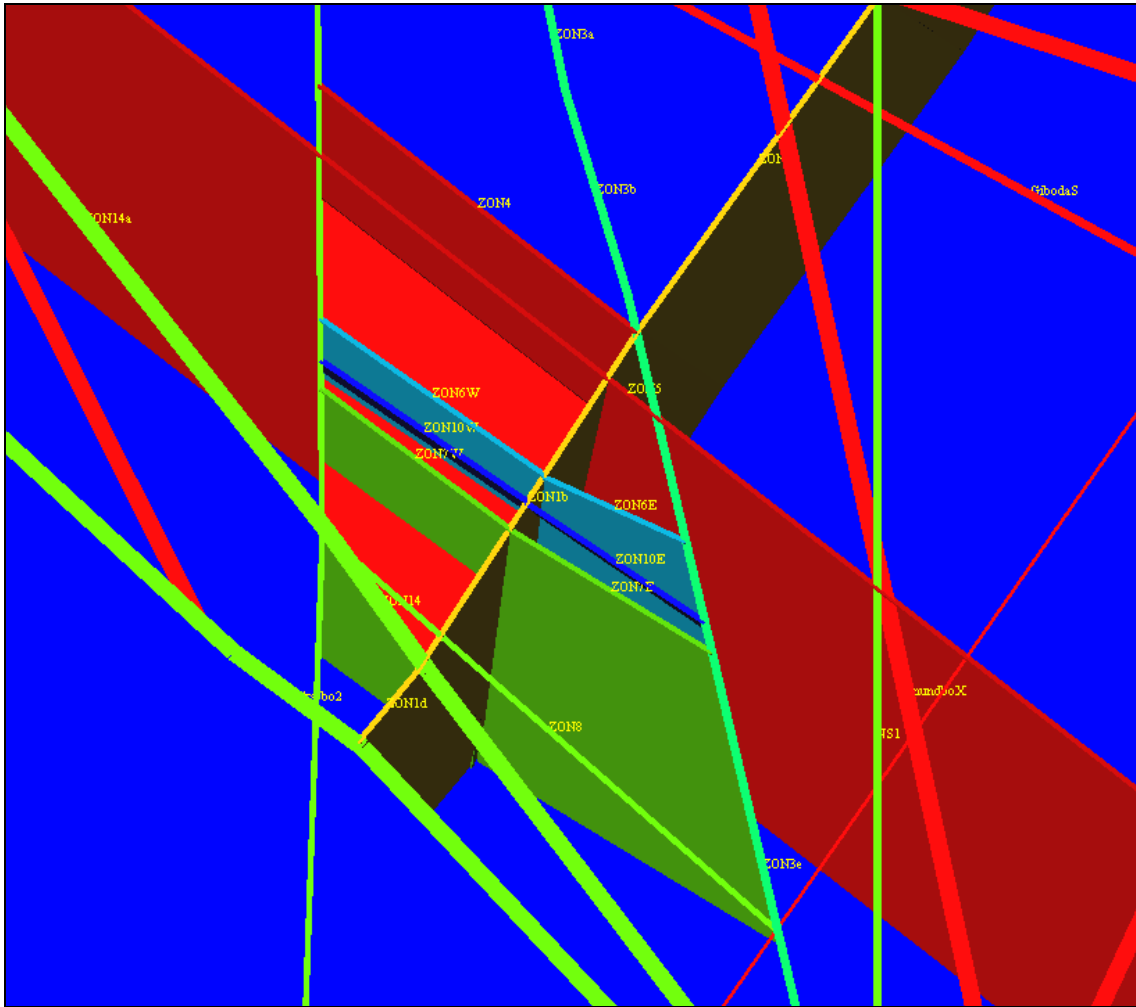
21

Figure 4-5   Plan view of the fracture zones in the site-scale model area. The fractures are coloured according to permeability. Red showing higher values and blue lower.
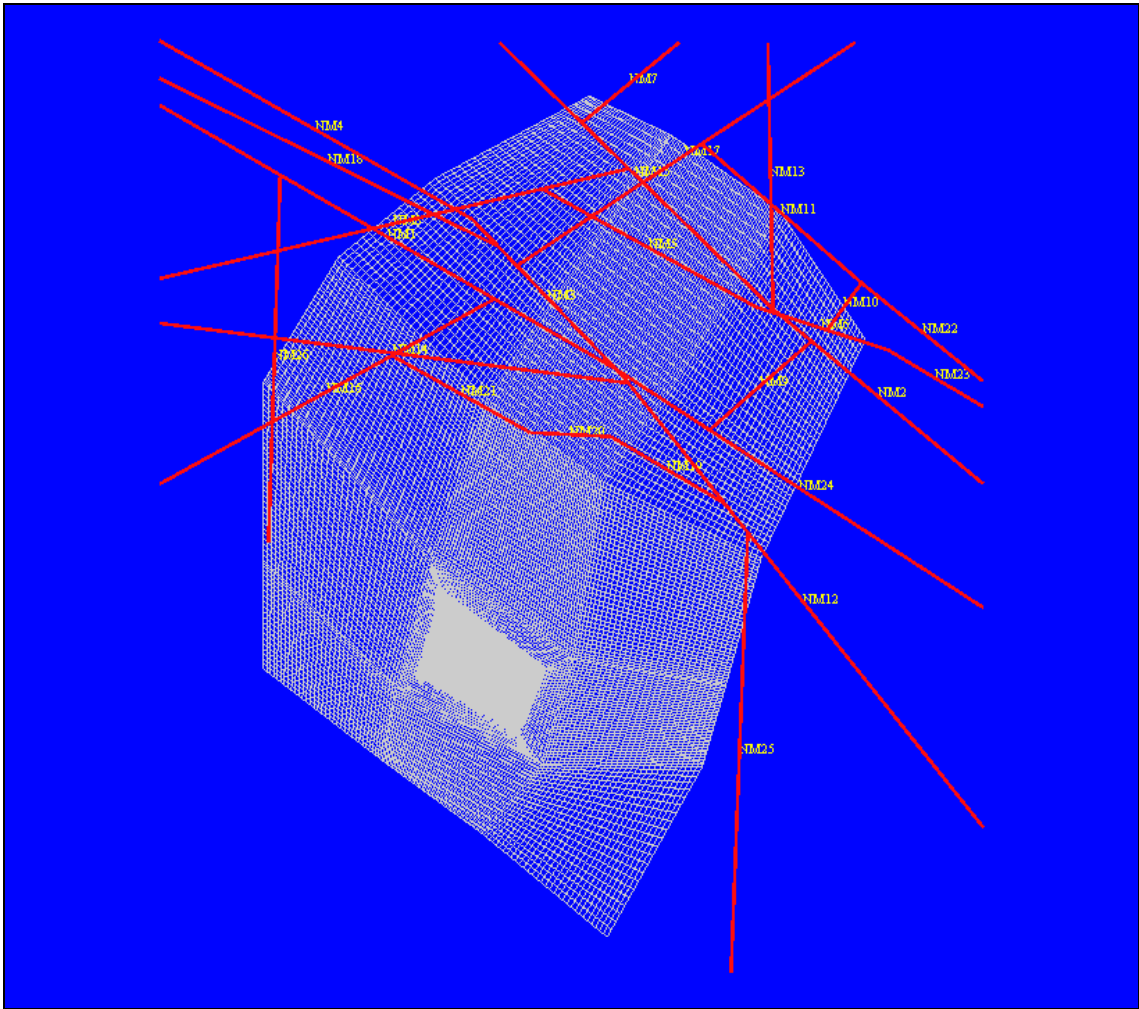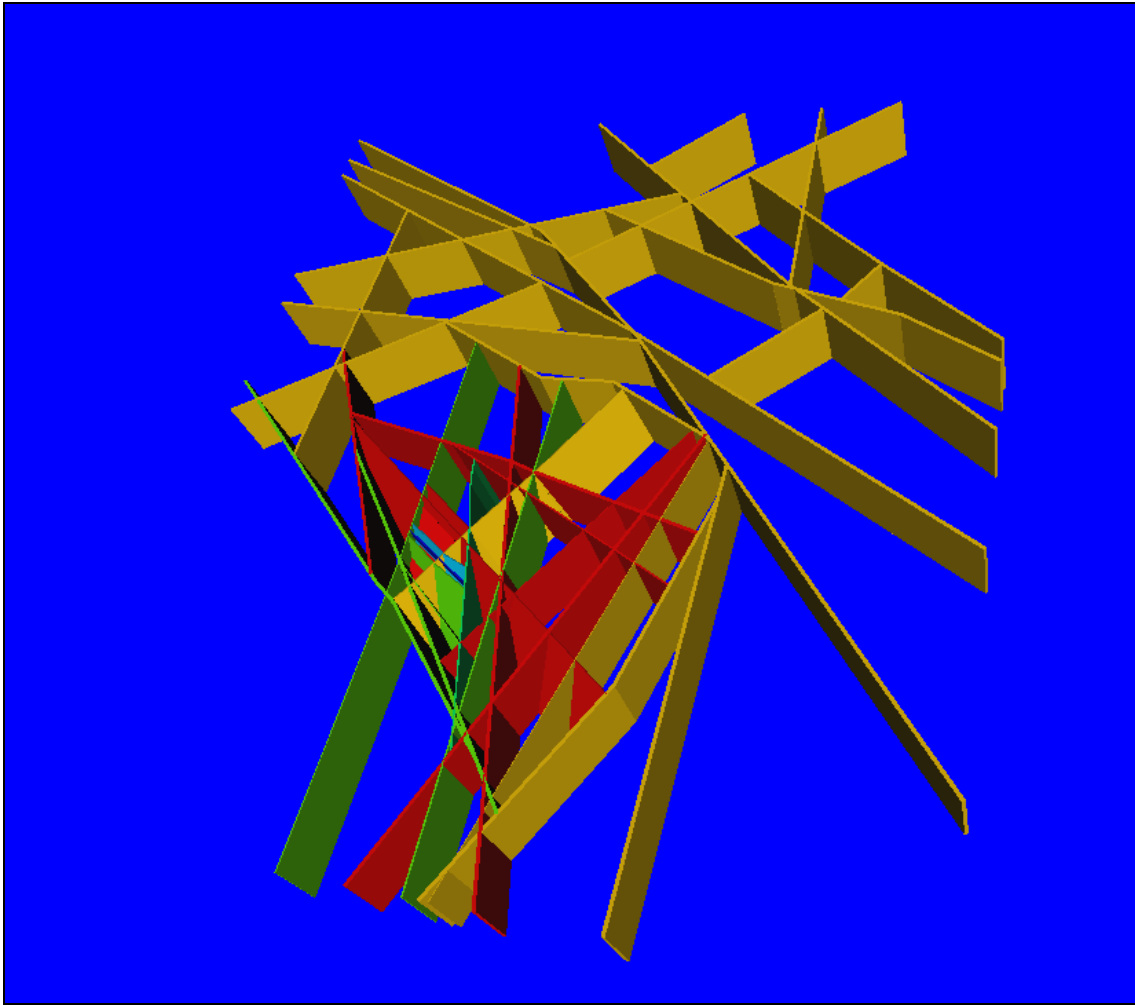
Figure 4-6   Plan view of the grid together with the new regional fracture zones.

Figure 4-7   Oblique view of all fracture zones as seen from the south-east and above. The fractures are coloured according to log10 permeability. Red showing higher values and blue lower.
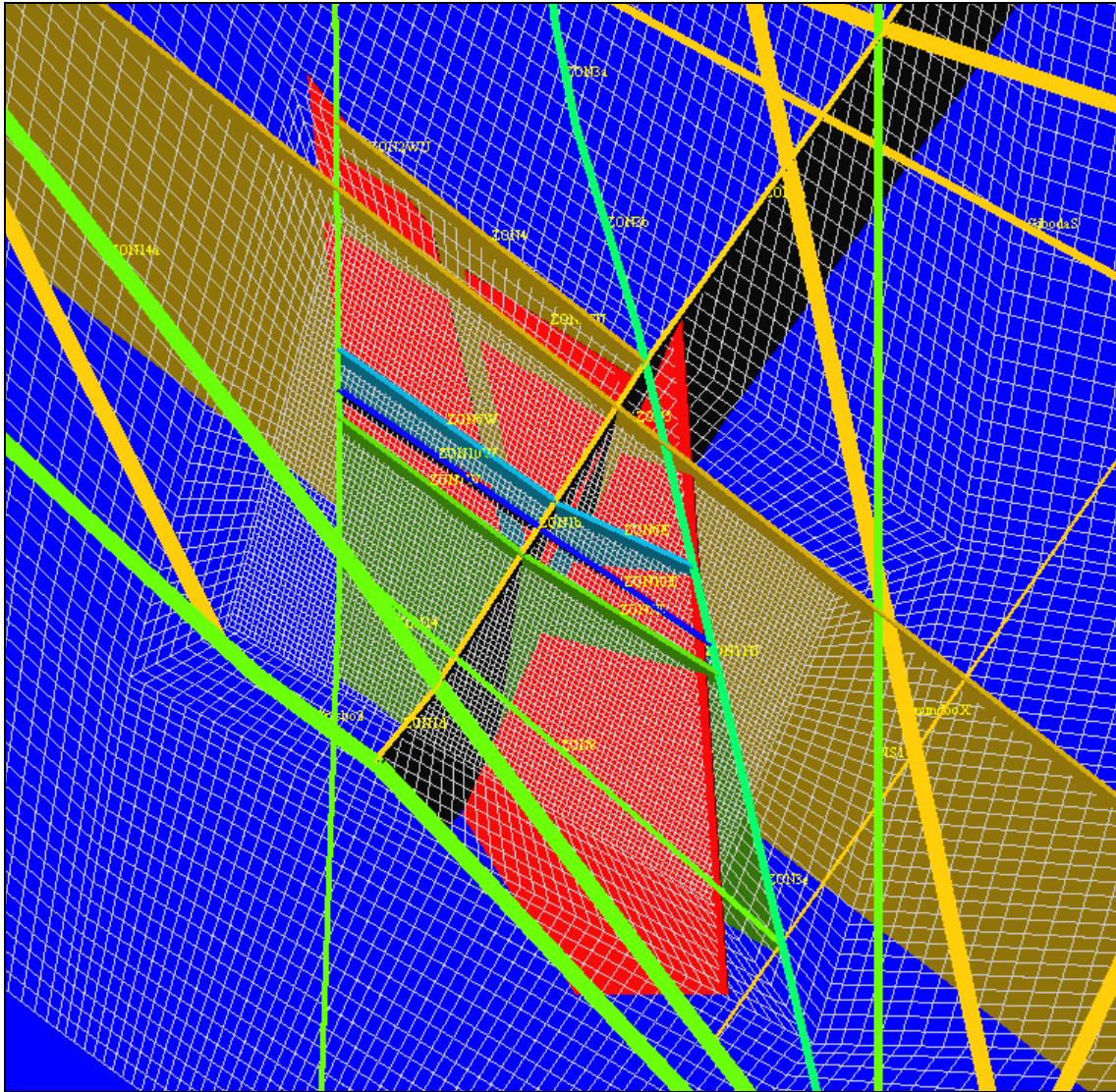
*Figure 4-8   Plan view of the grid and fracture zones zoomed in on the site-scale.
North is up the page.*

4.2   Parameterisation

The rock properties were defined in terms of three vertical layers: above 35m deep,
above 875m deep and below. Table 4-1 and Table 4-2 present the parameter values used
for each rock type in the NAMMU model. Extra rock types were introduced to
distinguish the regional- and local-scale regions. An extra intermediate-scale type was
added for the band of concentric refinement around the local-scale. Parameters were
different for the two scales based on upscaling of borehole flow logs to different mesh
scales. This is consistent with (Marsic *et al.*, 2001). The properties for the core regions
of Zone 2 and Zone 11 were used in some variants to model the scenario of a semi-
impermeable core that had been characterised in Andersson *et al.* (1991). The
permeability was chosen arbitrarily low at that of the base rock mass to illustrate its
potential effect.

| Rock Name	K_{XX} [m^2]	Log$_{10}$K [m^2] Spread	Element Scale [m]
RS rock-mass z>-35m	1.55E-14	0.46	100
RS rock-mass z>-875m	1.26E-15	0.32	100
RS rock-mass z<-875m	5.00E-16	0.32	100
LS rock-mass z>-35m	1.55E-15	0.83	35
LS rock-mass z>-875m	5.62E-16	0.83	35
LS rock-mass z<-875m	5.62E-16	0.83	35
IS rock-mass z>-35m	1.55E-14	0.46	70
IS rock-mass z>-875m	1.26E-15	0.32	70
IS rock-mass z<-875m	5.00E-16	0.32	70
Zone 2 core	5.00E-16	0.32	35
Zone 11 core	5.00E-16	0.32	35

Table 4-1   Rock type permeabilities used in deterministic and stochastic models. Different rock types are used on the different element scales and in the depth zonation. RS denotes the regional-scale, LS the local-scale and IS the intermediate-scale. The base permeability before the fracture zones are included is isotropic and given by K_{xx}.

Rock Name	Porosity	Specific storage coefficient [1/m]t	Longitudinal dispersion length [m]	Transverse dispersion length [m]	Tortousity
RS rock-mass z>-35m	2.00E-02	1.00E-10	80	40	1.00
RS rock-mass z>-875m	2.00E-02	1.00E-11	80	40	1.00
RS rock-mass z<-875m	2.00E-02	1.00E-11	80	40	1.00
LS rock-mass z>-35m	2.00E-02	1.00E-10	30	15	1.00
LS rock-mass z>-875m	2.00E-02	1.00E-11	30	15	1.00
LS rock-mass z<-875m	2.00E-02	1.00E-11	30	15	1.00
IS rock-mass z>-35m	2.00E-02	1.00E-10	60	30	1.00
IS rock-mass z>-875m	2.00E-02	1.00E-11	60	30	1.00
IS rock-mass z<-875m	2.00E-02	1.00E-11	60	30	1.00
Zone 2 core	2.00E-02	1.00E-11	30	15	1.00
Zone 11 core	2.00E-02	1.00E-11	30	15	1.00

Table 4-2   Rock type properties used in deterministic and stochastic models. Different rock types are used on the different element scales and in the depth zonation. RS denotes the regional-scale, LS the local-scale and IS the intermediate-scale.

26

The total porosity value used for the rock mass was 2% as was the case in SR 97. This value originated from laboratory diffusion tests, but was also shown to give an evolution of the regional salinity in SR 97 at about the correct rate to match the deep borehole data. A total porosity of 5% was used for all fracture zones. Some specific storage values were available (Andersson et al., 1991), these were augmented by values used in SR 97. Generally, for the range of values available this is not an important parameter for long natural transients as hydraulic diffusion takes place on shorter time scales than the movement of salt. The dispersion parameters were chosen to be about the element-size for longitudinal, and half for transverse. These are about the smallest values that can be used without risking numerical Peclet number problems.

Figure 4-9 shows the permeability field on the surface of the embedded model after applying IFZ for all fracture zones. Figure 4-10 shows the permeability field on the local-scale and on the interface between the regional- and local-scales.
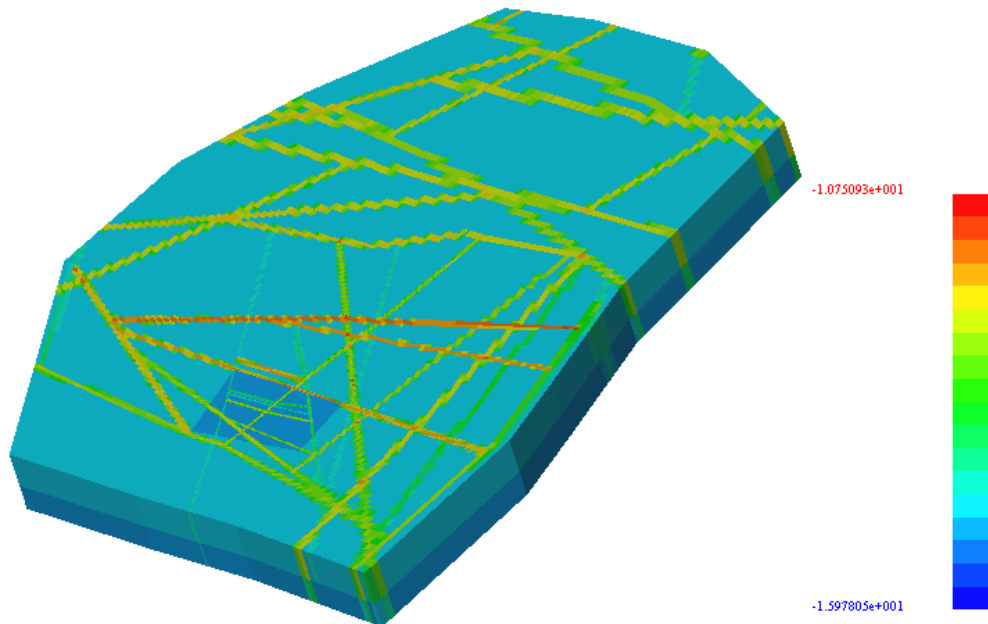
Figure 4-9   Oblique view of the effective permeability field as seen from the south-east and above. The elements are coloured according to permeability. Red showing higher values and blue lower.
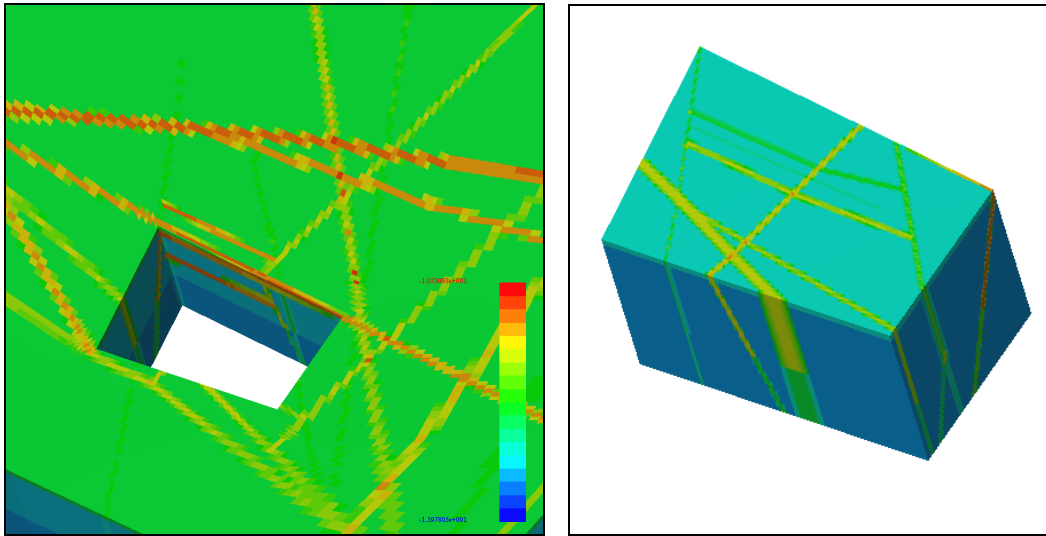
Figure 4-10   *Oblique view of the effective permeability field on the regional scale as seen from the south-east and above. Regional scale (left) and the site-scale (right). The elements are coloured according to permeability. Red showing higher values and blue lower.*

4.3   Time-steps and CPU usage

A fully implicit Crank-Nicholson time stepping scheme was used. In total 99 time-steps were used per run. Initially, small time-steps were used to resolve early fast transients in the major fracture zones. Time-step sizes were then gradually increased until a final constant time-step of 250 years was used. Each transient simulation used approximately 700 - 800 MB of RAM. When running on a Sun Enterprise 450 ($4 \times$ UltraSPARC-II 400MHz) computer, each run took about 30 to 35 hours to complete. This compares with the execution times on an Intel PIII 900MHz equipped PC running Linux, which were approximately 40% lower.

Time interval (year)	Real time [year]	Time step size [yrs]	Nr of time steps
0 - 16	3986 BP	2	8
16 - 40	3960 BP	4	6
40 - 200	3800 BP	10	16
200 - 400	3600 BP	20	10
400 - 1800	2200 BP	50	28
1800 - 4000	Now	200	11
4000 - 9000	5000 AP	250	20

Table 4-3   *Time steps used for the transient simulations.*

4.4   Transient results

The evolution of residual pressure and salinity on the top surface of the model from 3900BP to 5000AP is shown in Figure 4-11 and Figure 4-12, respectively. At the beginning most of the model is beneath the Litorina sea apart from a few islands in the south-east. By 2000 BP the site region has started to lift above the sea, although Lake Finnsjön is still below sea-level. For the current situation, the whole model is above sea-level. In the future, although the residual pressure will continue to rise, the relative topographic head gradients will remain unchanged.

The salinity profiles shows that initially much of the model is saline, although there is already a reduction in salinity around the fracture zones as freshwater infiltrates them and mixes with the marine saline water. By 3000 BP the near-surface in the south has become fresh, and saline water is discharged through the top surface in the north. By 2000 BP most of the near-surface is fresh, and there are only a few places where saline water discharges through the top. The present day situation is that near-surface is almost totally freshwater, with just a very few small lake areas where weak saline water discharges to the surface. The flushing of salt water from the model continues, but is now out of the northern side of the model. This illustrates how the system evolves in time and reinforces how flexible boundary conditions have to be applied to simulate such behaviour over long transients on the regional-scale.

Figure 4-11   Residual pressure at the top boundary of the model at different times: (a) 3900 BP, (b) 2000 BP, (c) Present time, (d) 1000 AP and (e) 5000 AP respectively. Range in head values shown are from 0 m to 86 m.
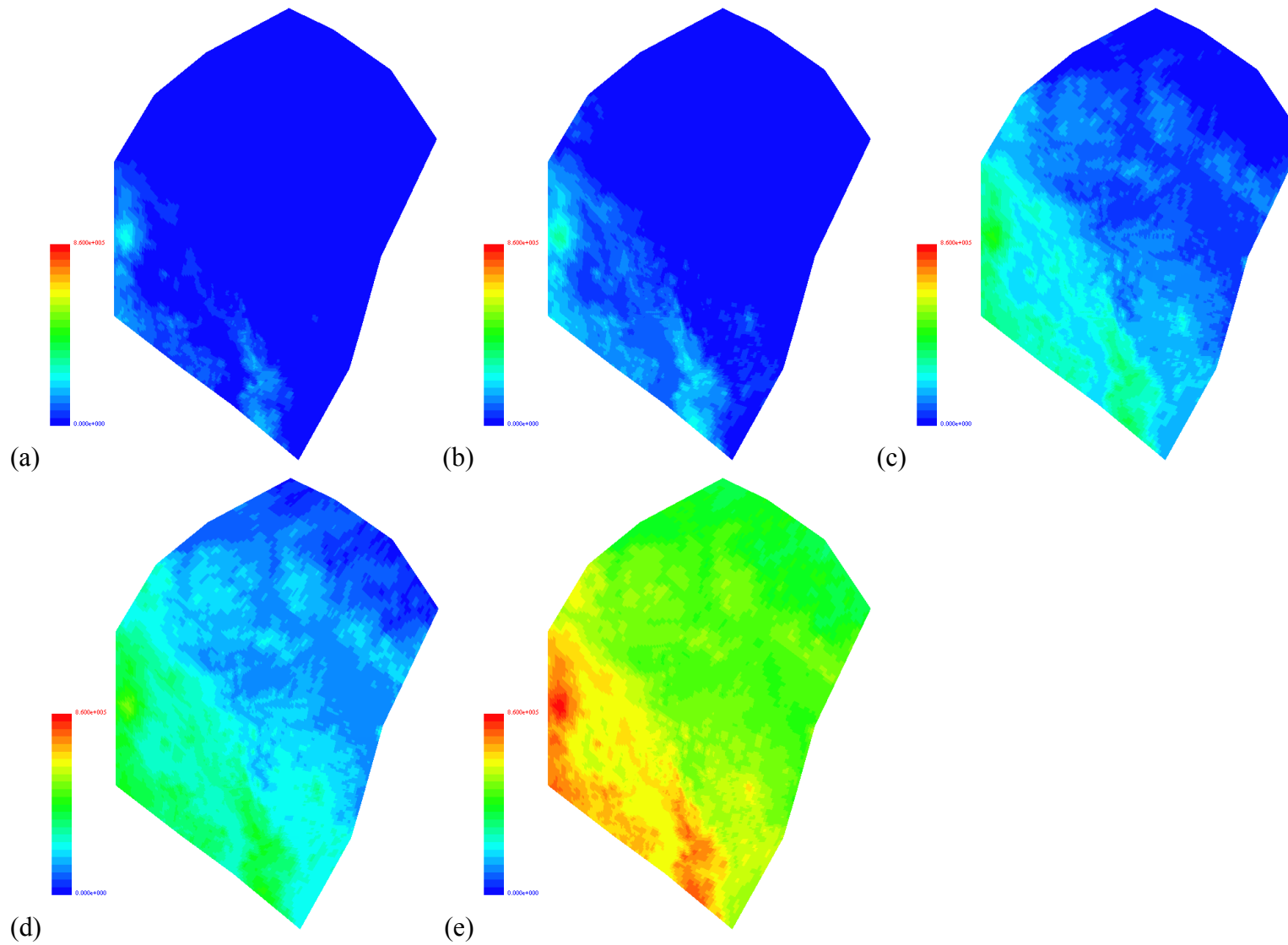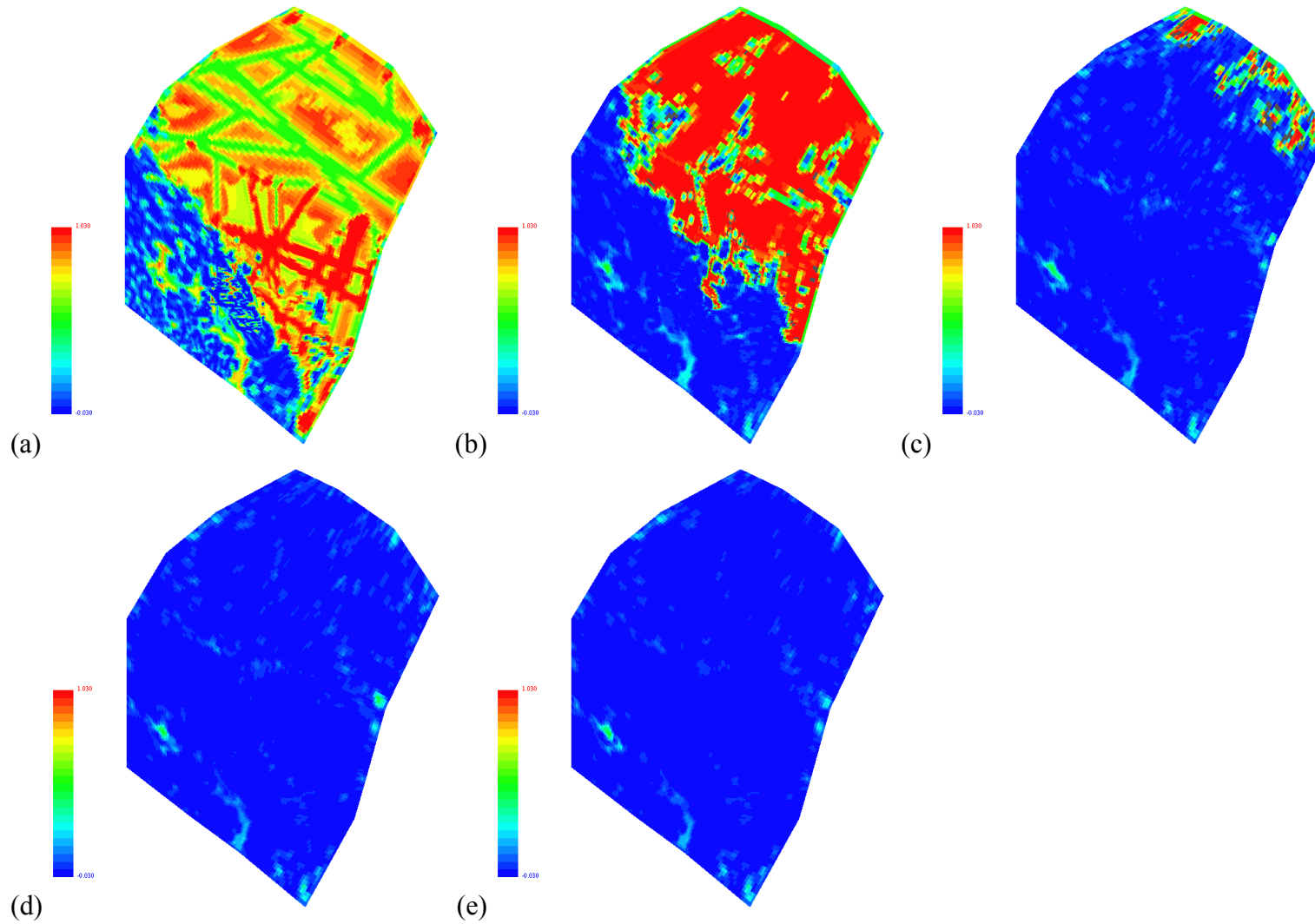
Figure 4-12   Salt concentration at the top boundary of the model at different times: (a) 3900 BP, (b) 2000 BP, (c) Present time, (d) 1000 AP and (e) 5000 AP respectively. Range in concentration values shown are from 0 to 1.

5 Calibration, variants and transport statistics

An important goal in this application was to establish whether the conclusions made in the SR 97 regional model on what parameters and structural features were required to obtain a match to the salinity measured in deep boreholes were still valid for this more refined model. Figure 5-1 shows the position of the deep boreholes for which salinity data was available. A match against pressure data was not performed, since it was considered that the salinity data provided a much more sensitive test for the calibration, especially given the low topography of the site.

The most important issue in obtaining a match was the structural interpretation of Zone 2. The salinity in deep boreholes was far more sensitive to the representation of Zone 2 than to parameter changes such as permeability and porosity. Hence, the variants considered focussed mainly on different representations of Zone 2. Of secondary importance were the porosity and dispersion parameters that effect the rate of changes in time and thickness of the saline transition zone, respectively.

Generally, it was found that using the same porosities as for SR 97 gave a system that evolved at the same rate as before, such that the observed characteristics of low salinities in the southern block and moderate salinity below Zone 2 was reproduced. However, using IFZ with Zone 2 modelled as a single layered high permeability plane as defined in the SR 97 local-scale model gave the salinity below Zone 2 far deeper than observed in the boreholes. To obtain a better match a layered structure of thin high permeability layers above and below a low permeability core was considered as had previously been required to get a match in the SR 97 regional model. This improved the match with a shallower saline transition zone, but still did not show the sharp transitions seen in the boreholes at the right depth. The next step was to retain the layered structure, but use the fracture zone geometries for Zone 2 and Zone 11 (a more steeply dipping sub-horizontal zone in the Southern rock block) as characterised in Andersson *et al.* (1991). Figure 5-2 and Figure 5-3 shows a horizontal and vertical view of the permeable layers for this model. Zone 2 is split into an east and west parts with an offset. The salinity data is represented by drawing tetrahedra coloured according to measured salinity. Viewing this more precise structural model and salinity data in three-dimensions it is clear to see a strong correlation between salinity and the top of Zone 2. Groundwater above Zone 2 is fresh, there is steep gradient across Zone 2, and then there is saline water below. This motivated using the original more complex structural interpretation of Zone 2.The picture in the Southern block is more complex. The groundwater below Zone 11 is moderately saline, but there is high salinity below the intersection of Zone 11 and Zone 3.

Table 5-1 lists the variants that were used to study the effect of the structural model (Cases 1, 2, 3 and 5), salinity (Cases 1+1f and 3+3f), and heterogeneity (Case 4).

Variant	Description
Case 1	Original structural model as defined in SR 97.
Case 1f	A freshwater steady state simulation of Case 1.
Case 2	Zone 2 represented as a three layered structure using IFZ. Zones truncated against Zone 2.
Case 3	The Base Case. Zone 2 and Zone 11 as in Andersson *et al.* (1991). Using Rock Block facility.
Case 3f	A freshwater steady state simulation of Case 3.
Case 4	A stochastic simulation of Case 3 with 5 realisations.
Case 5	Based on Case 3 but with zones truncated against Zone 2.

Table 5-1   Brief description of the variants.

For each variant transport statistics for particles released from 120 canister locations were considered for comparison with other structural models and to SR 97. Statistics were calculated for travel times (TT), path lengths (PL) and canister fluxes (CF). Since some of released particles were stuck inside the model due to numerical problems these particles had to be removed when calculating the statistics for the travel time and the path lengths otherwise they would skew the results. The fraction of the released reaching the top boundary is presented in the statistical summaries. Particles not reaching above -100 m were excluded in the statistics for TT and PL. The statistics for the canister flux was based on the ensemble of 120 particles since the flux is measured at the starting position of the particle and therefore independent of the pathlines. The figures presenting exit locations for the different variants are based on the ensemble of 120 particles and consequently include any stuck particles.

The pathlines were based on starting particles at four different times, present, 1000 years AP, 3000 years AP and 4750 years AP and moving the particles in a snapshot of the flow field corresponding to the start time. The reason for this was to quantify the uncertainties in transport statistics relating to release time. Although it would be possible to calculate pathlines moving in a time-varying flow-field, such calculations would require an accurate model of transport porosity in the rock mass and fractures to have any meaning. A uniform transport porosity of 10^{-4} was used throughout this study. This is same value as was used with in the SR 97 study, hence the transport statistics presented in Table 5-6 and Table 5-7 are fully comparable. It would be interesting in the future to consider pathlines in a time-varying flow-field. However, it does raise difficulties in terms of interpretation, at what time to release particles, and having to calculate the flow-field for sufficient time in to the future for all particles to exit.
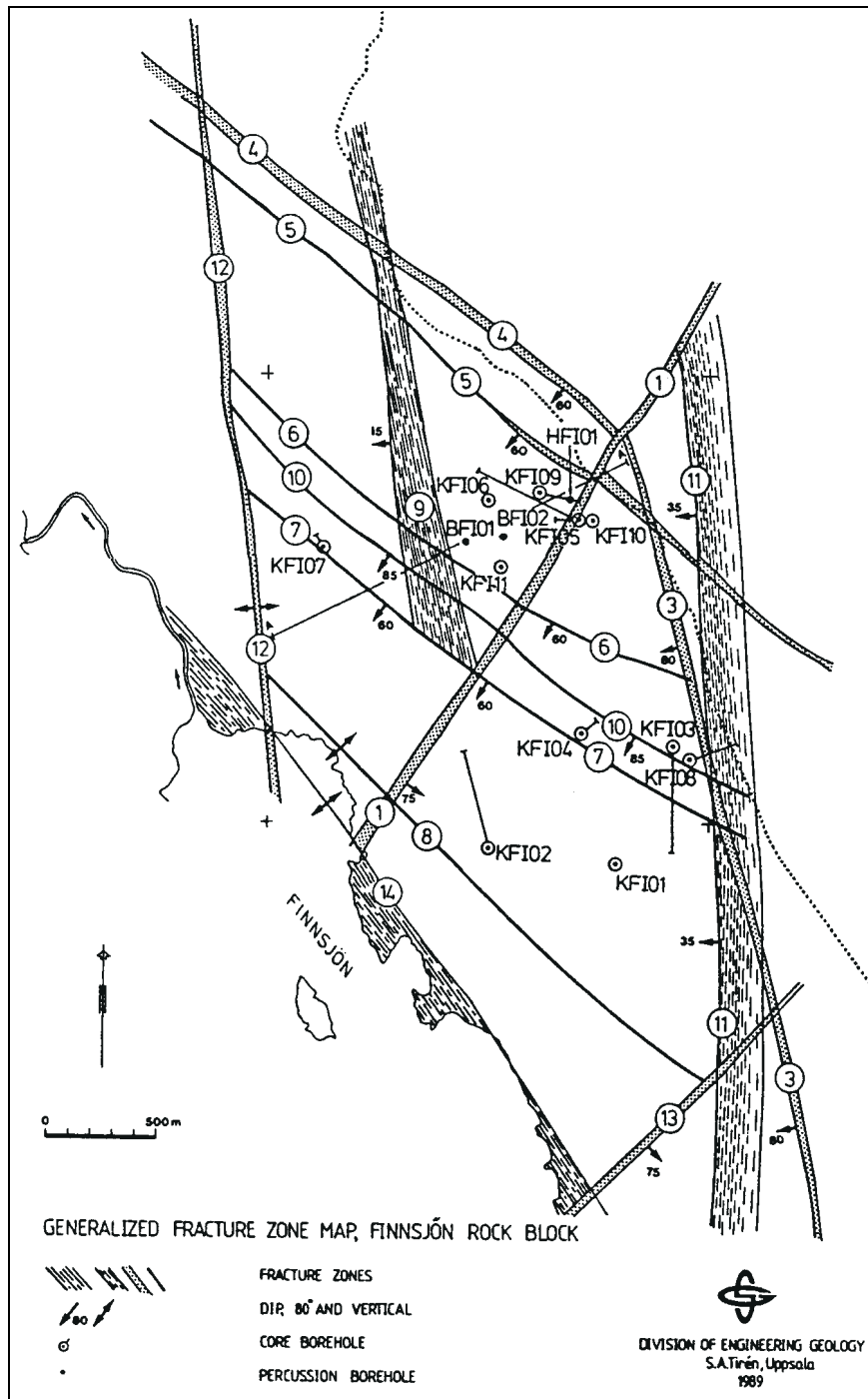
*Figure 5-1   Map of fracture zones and boreholes in the vicinity of the Finnsjön
rock block. Reproduced from Andersson et al. (1991).*

Figure 5-2 *Zoomed in visualisation of measured salinity in deep bore holes shown as coloured tetrehedra (blue: <500mg/l Cl; green: <2000mg/l Cl; red>2000mg/l Cl). The view shown is at repository depth looking from south to north. The vertical zones are Zone 1 (yellow), Zone 4(yellow, left side) and Zone 3 (green). The sub horizontal zones are Zone 2 (red, split into four parts on the left side) and Zone 11 (red, two parts on the right side).*
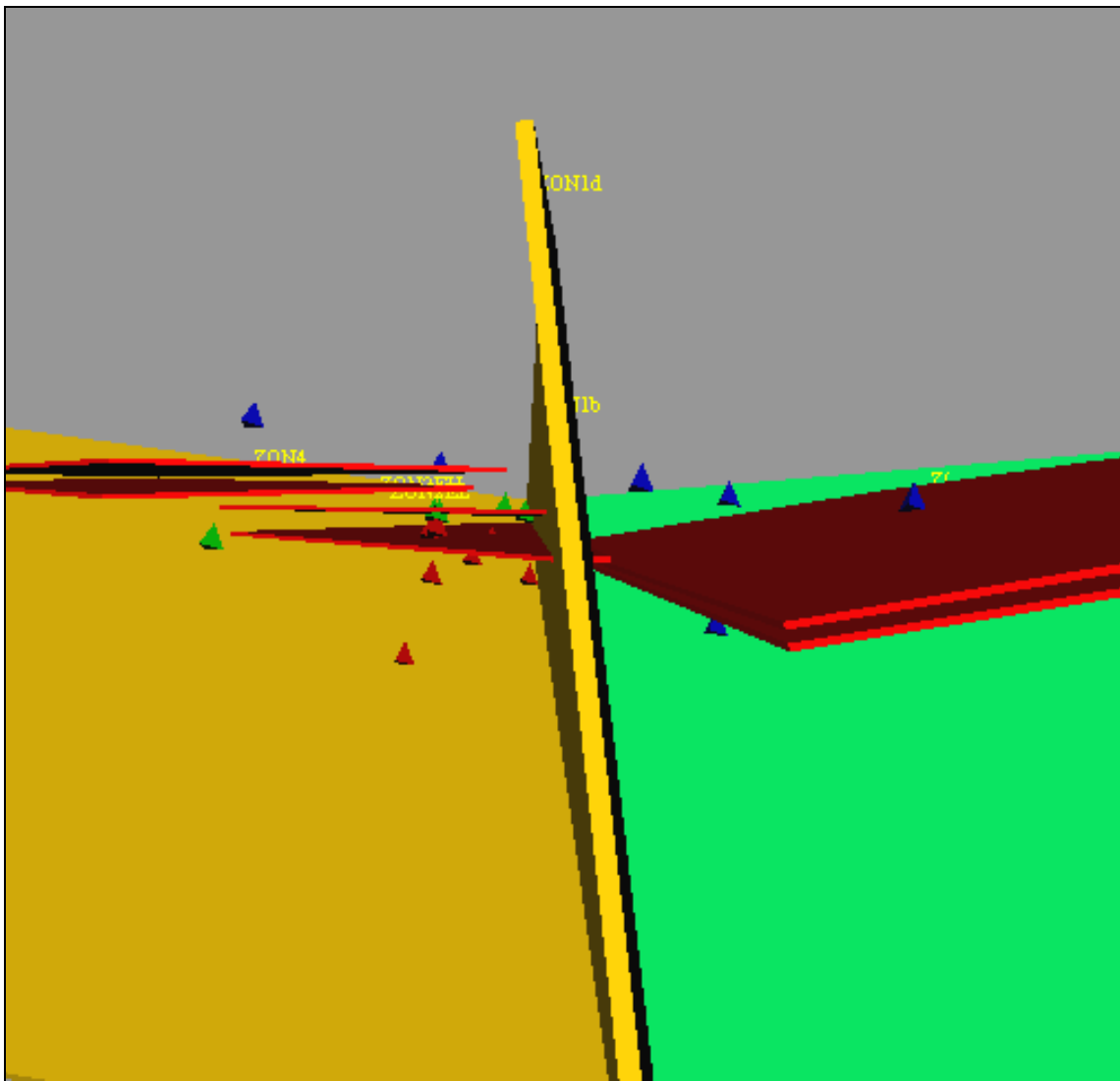
Figure 5-3   *Zoomed in visualisation of measured salinity in deep bore holes shown as small coloured tetrehedra (blue: <500mg/l Cl; green: <2000mg/l Cl; red>2000mg/l Cl). The view shown is from above. North is up the page. The vertical zones are Zone 1 (yellow), Zone 4(yellow, left side) and Zone 3 (green). The sub horizontal zones are Zone 2 (red, split into four parts on the left side) and Zone 11 (red, two parts on the right side).*
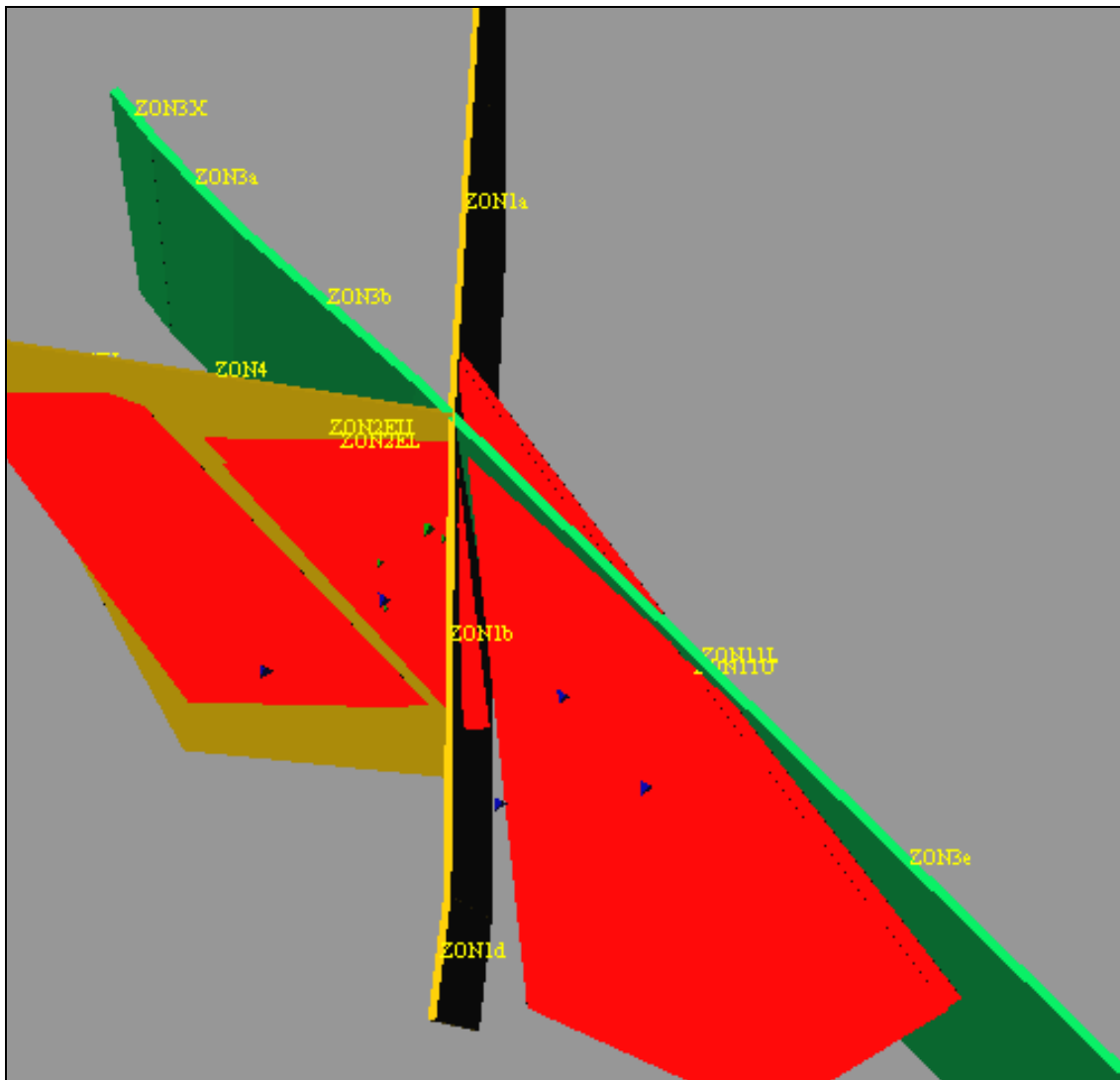
5.1   Case 1

Case 1 is the original structural model and properties as used in Marsic *et al.* (2001). Figure 5-4 shows the predicted salinity contours together with the permeability field on three vertical slices along a-A, b-B and c-C, see Figure 5-1. The contours of salinity correspond to 5%, 25%, 50%, 75% and 95% of the maximum salinity (corresponding to 6500 mg/l). The 5% contour is the one that is closest to the top of the model and the 95% is the one closest to the bottom of model. The profiles are shown for present day conditions. Note the vertical scale is exaggerated by a factor of two. Slice a-A cuts through the northern rock block (and Zone 2) in a south-north direction. Some of the observed characteristics with relatively high salinity below Zone 2 have been reproduced but the transition is not as sharp as the measurement data indicate. The effect of infiltrating freshwater flushing out the saline water through the fractures is clearly apparent. In slices b-B (cuts through the southern rock block SSW-NNE) and c-C (cuts NW-SE through both rock blocks) the lower salinity in the southern rock block can be seen. Note that Zone 11 is not present in Case 1. This zone probably has great effect on the complex salinity conditions in the southern rock block.
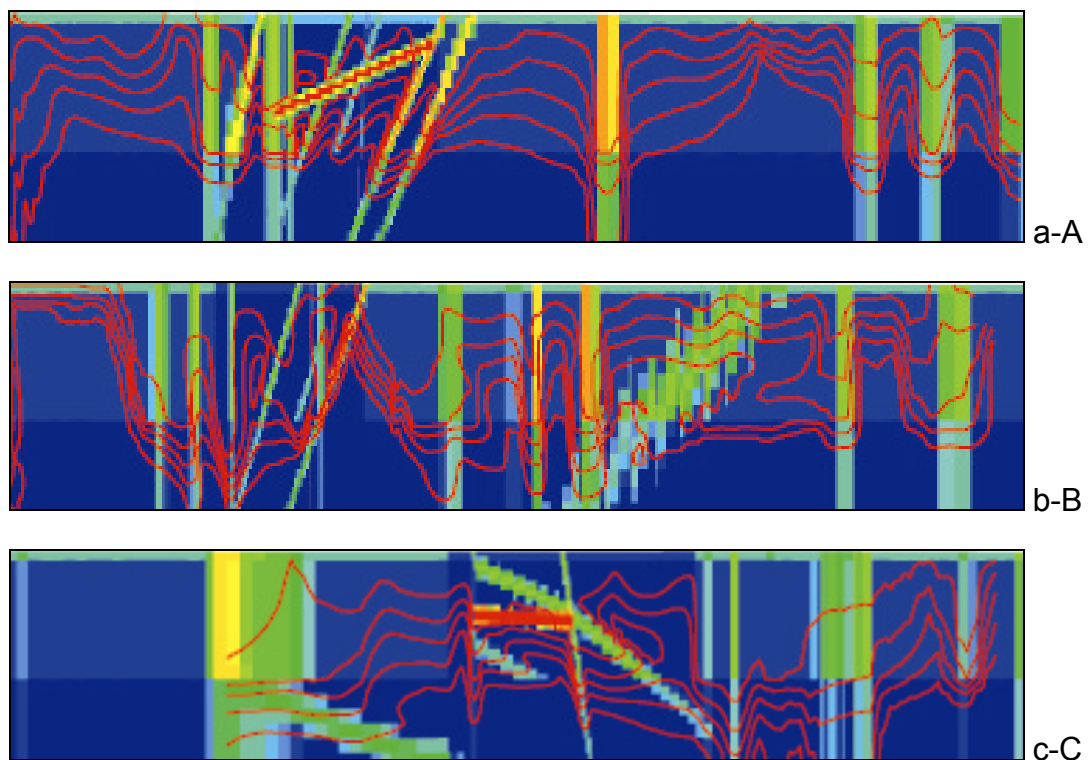
Figure 5-4   *Salinity for Case 1 shown on vertical slices coloured according to the logarithm of permeability along* a-A*,* b-B *and* c-C*, see Figure 5-1. The contours of salinity correspond to 5%, 25%, 50%, 75% and 95% of the maximum salinity (corresponding to 6500 mg/l). Note the vertical scale is exaggerated by a factor of two.*

Figure 5-5 shows the predicted salinity profiles in the deep boreholes along with the measured values. Profiles are shown for the boreholes BFI01, KFI04, KFI06 and KFI07, see Figure 5-1. These are four of the deeper site boreholes and are spread over a large area of the site. KFI04 is in the southern rock block while the others are in the northern rock block. KFI04 and KFI07 calibrate quite well. The model prediction of salinity below Zone 2 in the northern rock block is far too deep and does not show the observed sharp transition, as can be seen for BFI01 and KFI06. Hence, it was judged that this case did not calibrate based on the original structural model used.

Since the structural model used in this model corresponds to that specified for SR 97, transport statistics were calculated for comparison with SR 97 and other structural models. Figure 5-6 - Figure 5-8 present the exit locations for the particles in the variable density simulation of Case 1 and the corresponding freshwater simulation, Case 1f. As can be seen, the exit locations are limited to Zone 5 and the Imundbo Zone. In SR 97, the Imundbo Zone was a very important feature since it corresponded to a majority of the exit locations. It should be noted that the difference between the two simulations is very small when it comes to exit locations.

In Table 5-2 a statistical summary for 120 starting positions for Case 1 is presented. In the summary, statistics for particles released at four different times in the variable density simulation is presented together with the results for the freshwater simulation. Two facts are worth noting; first, the difference made by releasing the particles at different times does have a noticeable effect on the performance measures. Second, as expected the saline simulation gives longer travel times and longer paths. Part of the explanation to the first point is that the saltwater is being pushed out of the fractures at an early stage leaving fractures filled with freshwater at constant conditions. The water in the rock mass between the fractures however is still saline and not changing much in time. Even if there are changes in velocity locally in the rock mass, the overall changes will be small because of the constant conditions in the fracture zones.
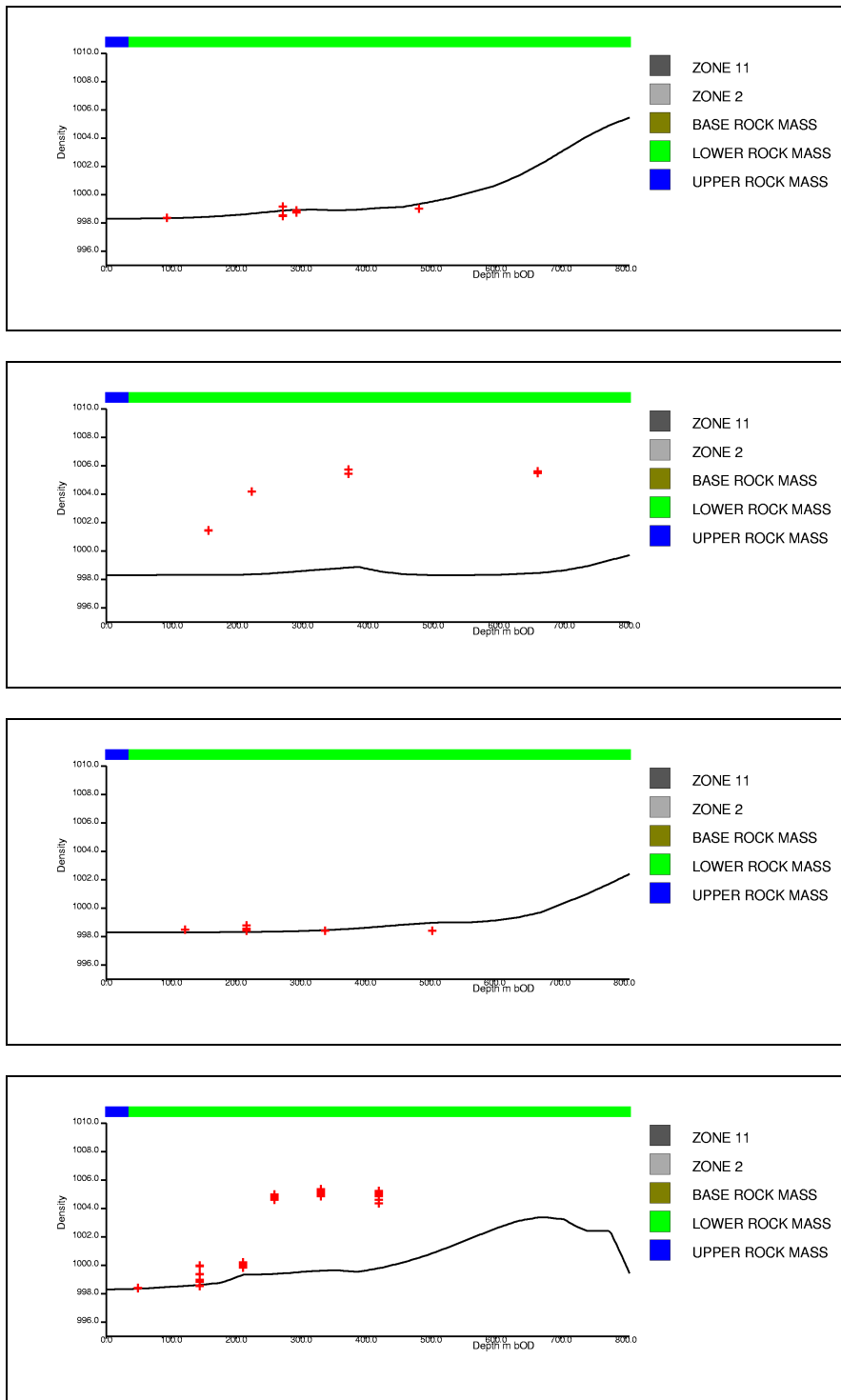
Figure 5-5   Salinity in the boreholes BFI01, KFI04, KFI06 and KFI07 (from bottom to top) for Case 1, see Figure 5-1. The solid lines represent the model results. The red crosses are experimental data. The depth of the model is shown on the x-axis with the top to the left. The range of density shown on vertical axis is 996 to 1010 kgm^{-3}.
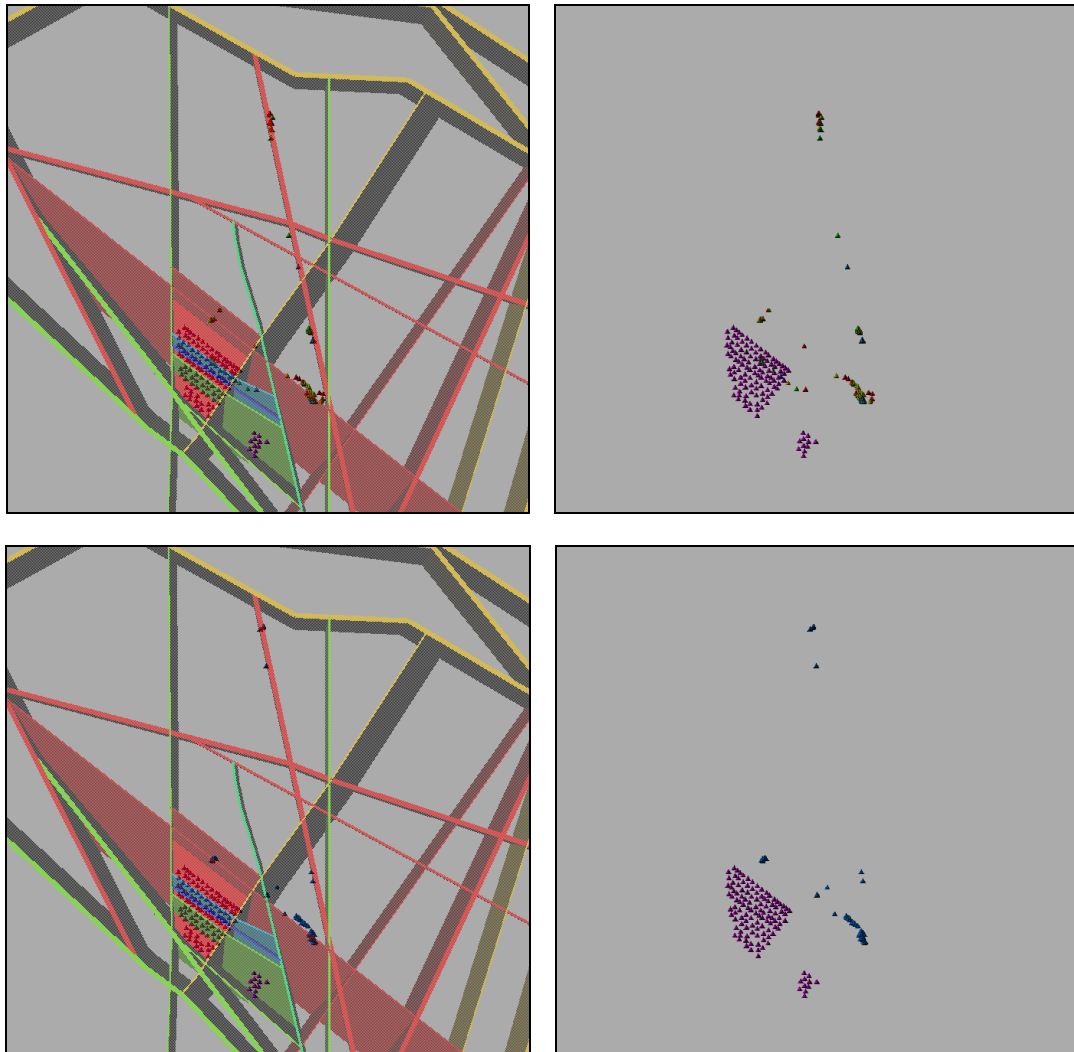
Figure 5-6   *Exit locations (blue markers) for Case 1 shown together with the starting positions (purple markers). Fracture zones removed for clarity in the pictures on the right side. <u>Top</u>: Variable density simulation. <u>Bottom</u>: Freshwater simulation (Case 1f).*
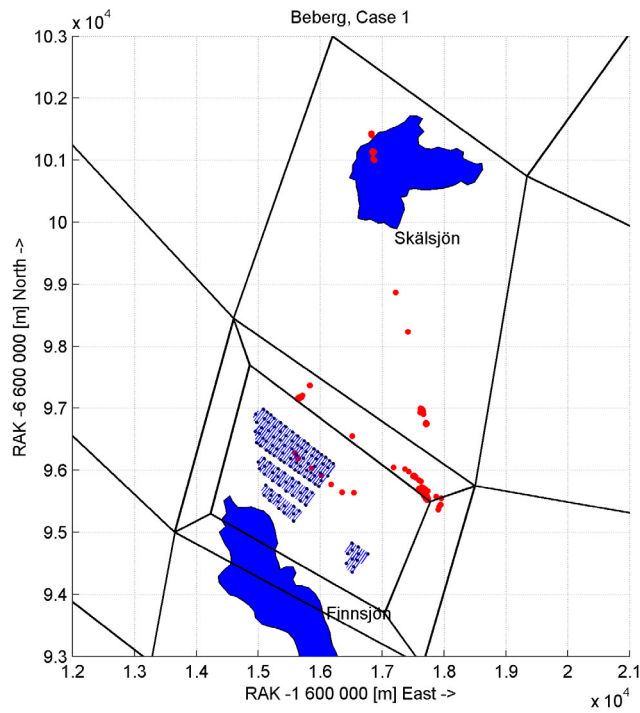
Figure 5-7   *Exit locations (red markers) for Case 1 (variable density simulation) shown together with the starting positions (black markers). The patch grid and some surface features have been included for orientation.*

Figure 5-8   *Exit locations (red markers) for Case 1f (freshwater simulation) shown together with the starting positions (black markers). The patch grid and some surface features have been included for orientation.*
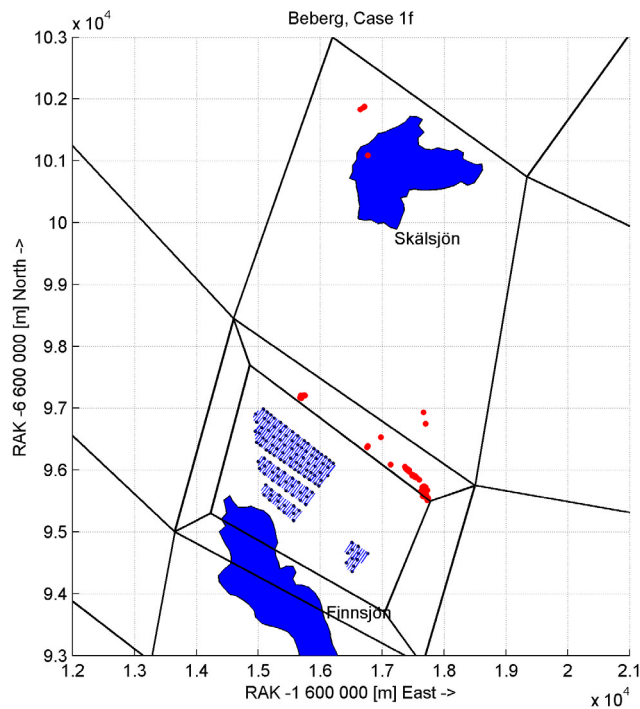
	Present time	1000 yrs	3000 yrs	4750 yrs	Freshwater
Log_{10}(TT *[yrs]*)					
Median	2.443	2.501	2.152	2.577	2.041
5th Percentile	0.607	1.041	0.756	0.970	0.917
25th Percentile	1.627	1.709	1.645	1.751	1.576
75th Percentile	2.589	2.820	2.749	2.694	2.418
95th Percentile	2.985	3.258	3.041	2.906	2.707
Variance	0.544	0.529	0.581	0.486	0.358
Fraction	0.992	0.958	0.942	0.900	0.967
Log_{10}(CF *[m/yr]*)					
Median	-3.099	-3.164	-3.245	-3.294	-3.520
5th Percentile	-3.777	-3.743	-3.827	-3.868	-4.116
25th Percentile	-3.301	-3.361	-3.464	-3.517	-3.835
75th Percentile	-2.919	-2.978	-3.073	-3.093	-3.174
95th Percentile	-2.690	-2.690	-2.710	-2.723	-2.737
Variance	0.335	0.338	0.376	0.394	0.483
Log_{10}(PL *[m]*)					
Median	3.731	3.762	3.616	3.756	3.533
5th Percentile	3.326	3.346	3.316	3.345	3.301
25th Percentile	3.494	3.534	3.468	3.506	3.437
75th Percentile	3.799	3.847	3.839	3.939	3.578
95th Percentile	3.949	4.111	4.114	4.028	3.815
Variance	0.039	0.052	0.064	0.055	0.018
Fraction	0.992	0.958	0.942	0.900	0.967

Table 5-2   Statistical summary for 120 starting positions for Case 1.

5.2   Case 2

In Case 2, an anisotropic representation of Zone 2 was used with a low permeable core surrounded by two high permeable fracture planes in a layered structure, see Figure 5-9. The structure, which was generated using IFZ, had a core (low permeability) thickness of 70 m while the two surrounding planes had a thickness of 15 m each.

In this variant, the zones surrounding or intersecting Zone 2 were truncated at a level exactly corresponding to the elevation of Zone 2. Consequently, zones 1b, 4, 5, 6W, 7W, 10W and 14 were truncated against the middle plane of the layered structure of Zone 2 (i.e. the original SR 97 interpretation of Zone 2), see Figure 5-9 and Figure 5-10.

The idea with this variant was to prevent the zones intersecting with Zone 2 to drain the salt from beneath Zone 2, hence the exact calculation of the intersections. However, it proved that the interpretation of Zone 2 as two displaced parts as in Case 3 had a larger effect on the model calibration. The transitions of salinity across Zone 2 were not as sharp as in Case 3 why it was judged that this case did not calibrate.
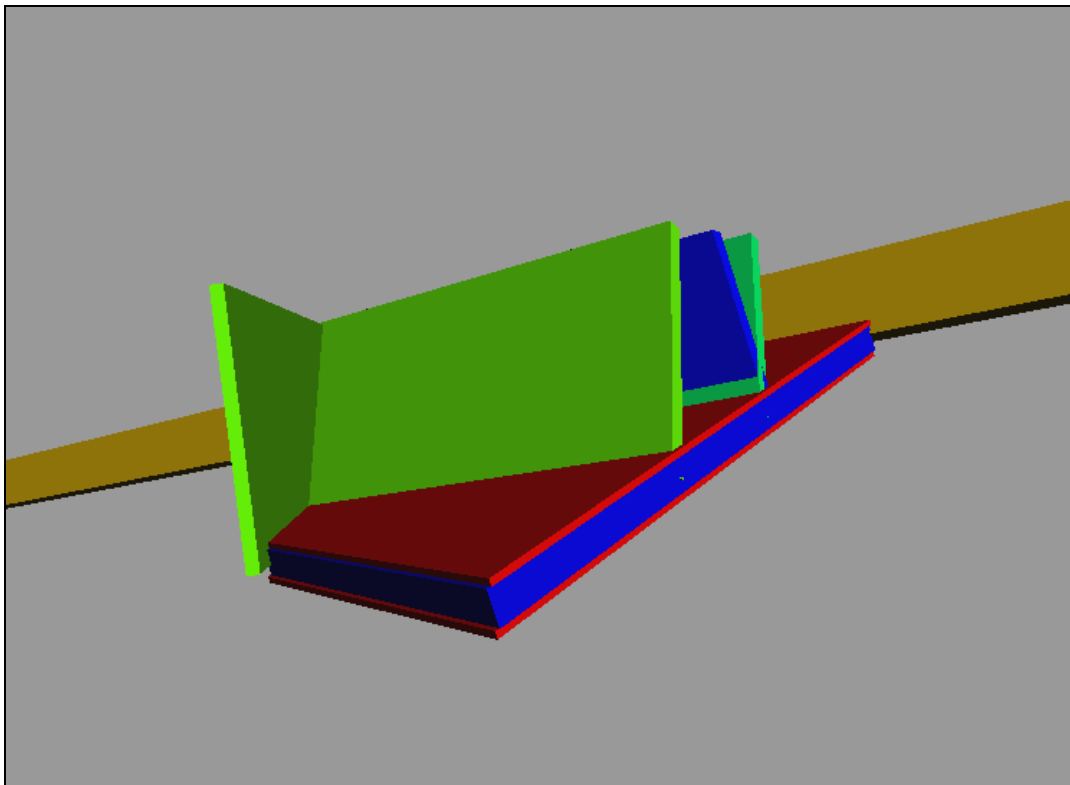
Figure 5-9   *Truncations of fractures surrounding or cutting through Zone 2.*
                    Layered structural representation of Zone 2 with a low permeable core
                    (blue) surrounded by two high permeable fracture planes (red).
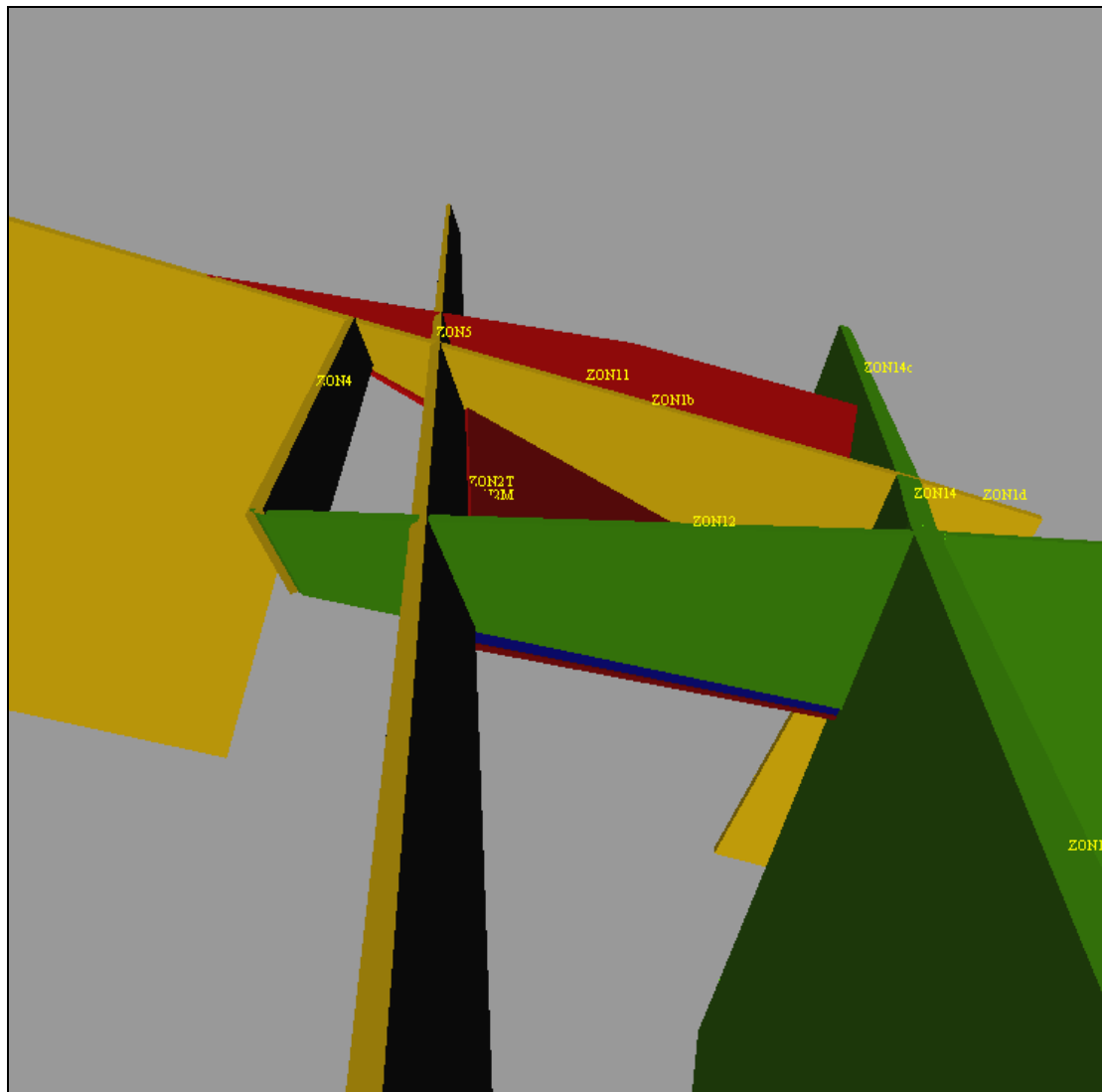
Figure 5-10   Truncations of fractures surrounding or cutting through Zone 2.

Figure 5-11 shows the predicted and observed salinity profiles for Case 2. Comparing to Case 1, there is now salinity at depth in BFI01 and KFI06, but it is deeper than the observed profile. Hence, it was judged that this representation of Zone 2 did not give a calibrated model, and so it was not relevant to calculate transport statistics. This lack of a match to salinity motivated consideration of the original and more complex interpretation of Zone 2 by Andersson et al. (1991).

Figure 5-11   Salinity in the boreholes BFI01, KFI04, KFI06 and KFI07 (from bottom to top) for Case 2, see Figure 5-1. The solid lines represent the model results. The red crosses are experimental data. The depth of the model is shown on the x-axis with the top to the left. The range of density shown on vertical axis is 996 to 1010 kgm^{-3}.
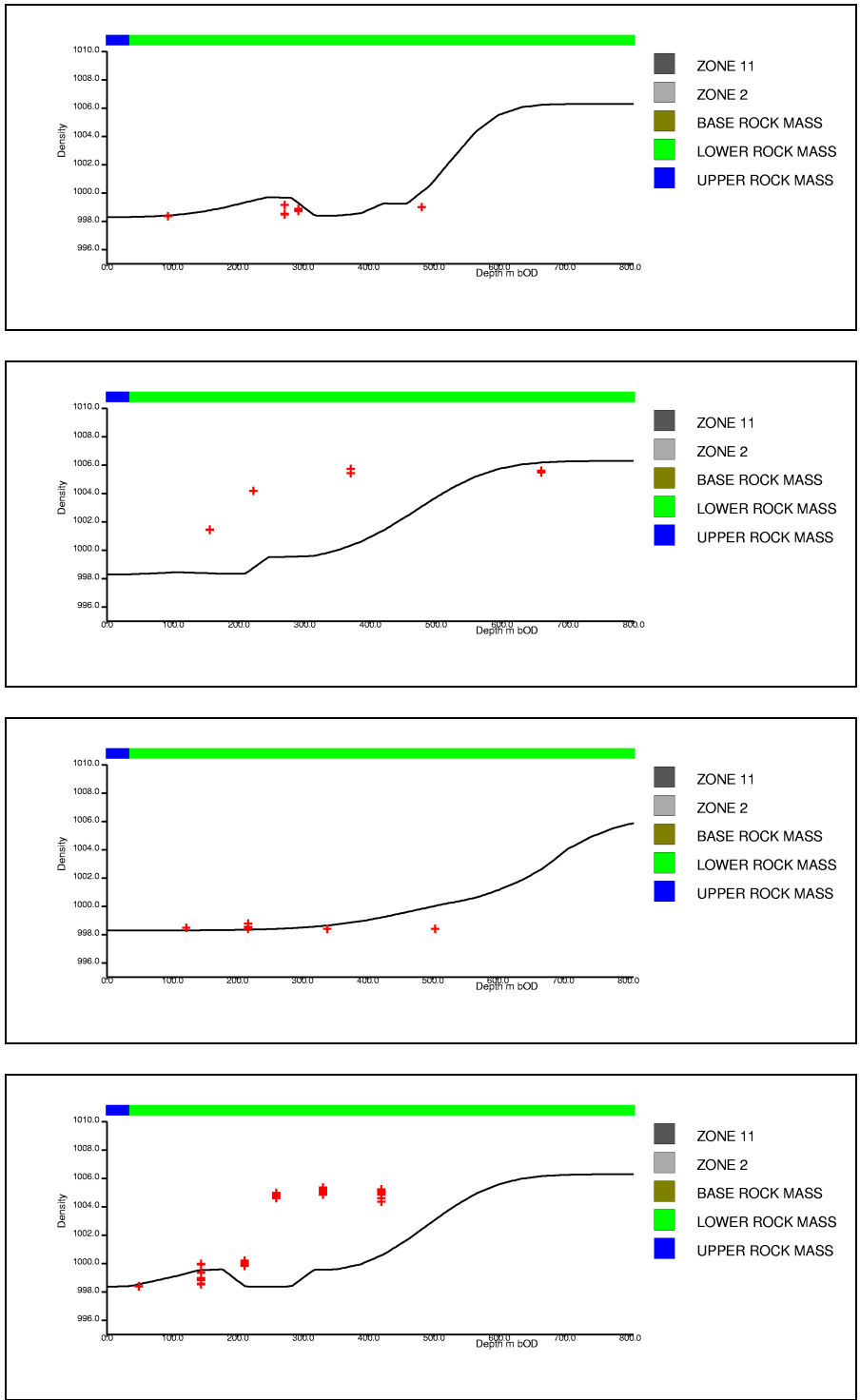
5.3   Case 3

In Case 3, Zone 2 is represented as in Andersson et al. (1991). This case was the first to give results that calibrated against the salinity data. Hence, for the purposes of comparison with SR 97, and other studies, it is referred to as the 'Base Case'. In Andersson et al. Zone 2 was interpreted as two parts (east and west) and each of them was split into an upper and a lower layer. Here, Zone 2 was modelled as a layered structure based on the geometry of Andersson et al. using a combination of the IFZ and rock block facilities. In Figure 5-12 the top left picture shows how Zone 2 (blue) and Zone 11 (yellow) are represented using the new Rock Block facility in NAMMU, see also Figure 5-13. The Rock Block facility changes the permeability inside a volume defined by planes. The top-right picture in Figure 5-12 shows the interpretation of Zone 2 (as in Case 2) and Zone 11 used by IFZ. In the bottom left and bottom right pictures the two different interpretations are superimposed to clearly show the differences in position of Zone 2.
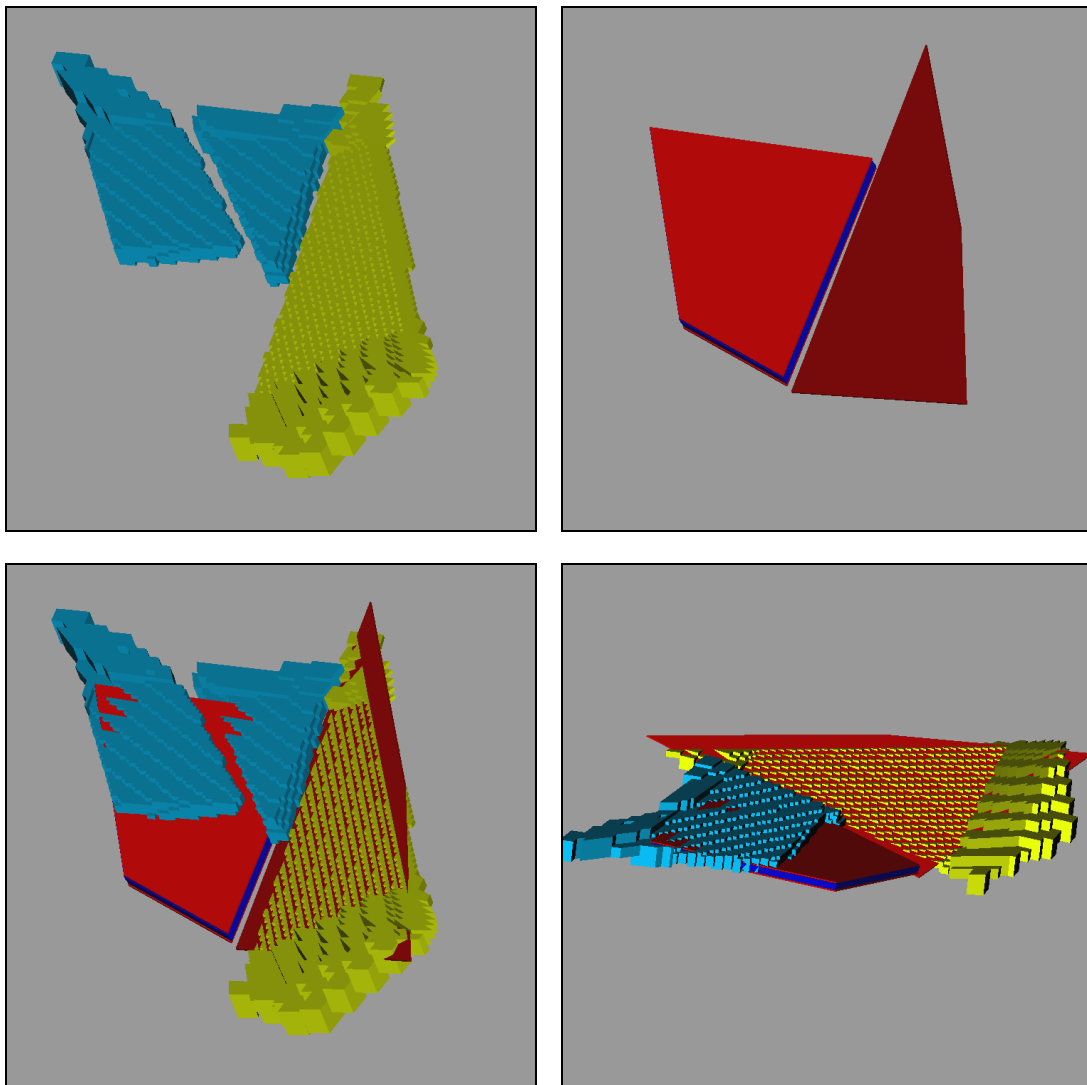

Figure 5-12   Different interpretations of Zone 2 and Zone 11. <u>Top-left</u>: The rock block facility used in NAMMU based on data from Andersson et al. (1991). <u>Top-right</u>: IFZ interpretation of the fractures. <u>Bottom</u>: Both approaches overlaid showing the differences.

These differences proved to have a great effect on the calibration of the model. Another change was made to the structural model of Case 3. The fracture zones cutting through Zone 2 (zones 1b, 4, 5, 6W, 7W, 10W, 14) were cut at a depth approximately corresponding to the elevation of Zone 2 (not exactly though since Zone 2 is sloping in all directions). This was done simply by changing the permeability of the fracture zones beneath the actual level to the background permeability of the rock.

Figure 5-14 shows the predicted salinity contours together with the permeability field on three vertical slices along a-A, b-B and c-C, see Figure 5-1. The contours of salinity correspond to 5%, 25%, 50%, 75% and 95% of the maximum salinity (corresponding to 6500 mg/l). The 5% contour is the one that is closest to the top of the model and the 95% is the one closest to the bottom of model. The profiles are shown for present day conditions. Note the vertical scale is exaggerated by a factor of two. Slice a-A cuts through the northern rock block (and Zone 2) in a south-north direction. In this variant, the relatively high salinity below Zone 2 have been reproduced and the transition is almost as sharp as the measurement data indicate. In fact, the model calibrates better than the rather coarse regional model of SR 97 and better than all the other variants in the present study. As in Case 1, the effect of infiltrating freshwater flushing out the saline water through the fractures is clearly apparent. In contrast to Case 1, Zone 11 is here included in the model. The result is a slightly higher salinity in the southern rock block but still lower compared to the northern rock block, see Figure 5-15. In slices b-B (cuts through the southern rock block SSW-NNE) and c-C (cuts NW-SE through both rock blocks) the lower salinity in the southern rock block can be seen. The complex conditions in the southern rock block have not been reproduced entirely only by including Zone 11 as in Andersson *et al.* (1991). However, the calibration can probably be improved considerably by revising the structural model. This conclusion also includes the northern rock block with Zone 2.
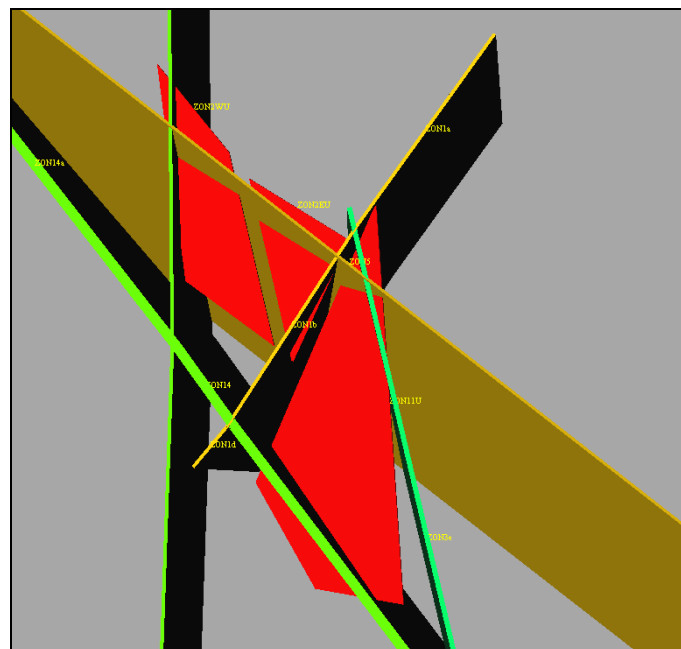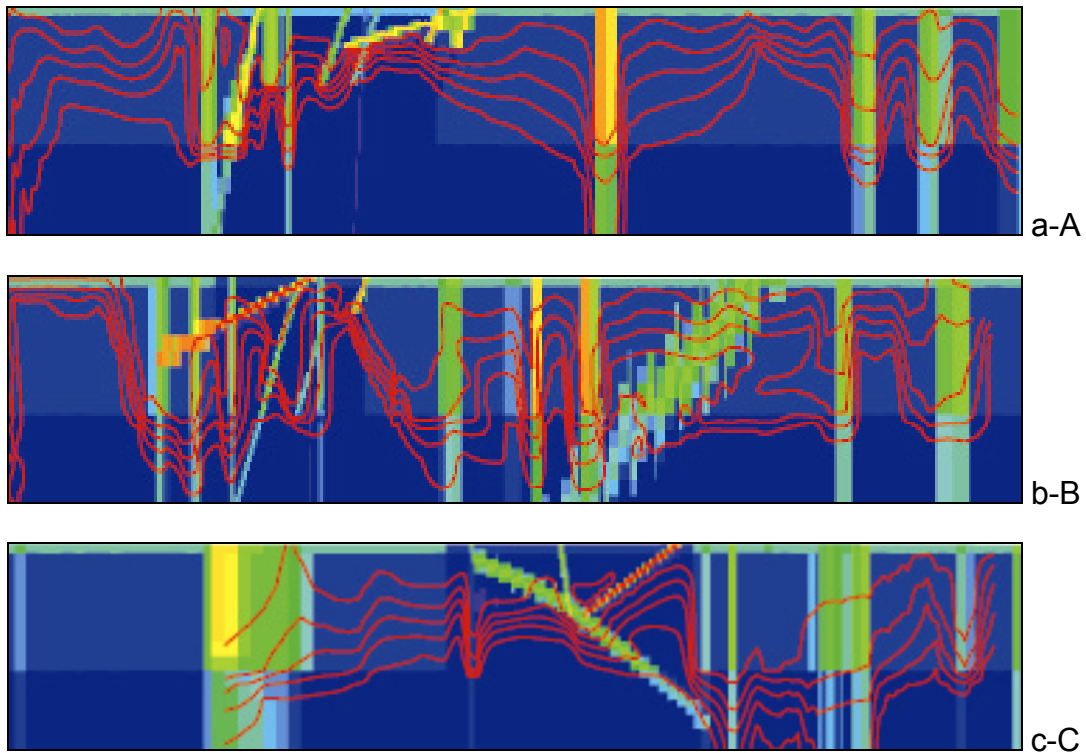

Figure 5-13   Plan view of Zone 2 (red, to the left) and Zone 11 (red, to the right) using data from Andersson et al. (1991). In NAMMU, a Rock Block facility was used to reproduce the zones.

Figure 5-14   *Salinity for Case 3 shown on vertical slices coloured according to the logarithm of permeability along **a-A**, **b-B** and **c-C**, see Figure 5-1. The contours of salinity correspond to 5%, 25%, 50%, 75% and 95% of the maximum salinity (corresponding to 6500 mg/l). Note the vertical scale is exaggerated by a factor of two.*

Figure 5-15 shows the predicted salinity profiles in the deep boreholes along with the measured values. Profiles are shown for the boreholes BFI01, KFI04, KFI06 and KFI07, see Figure 5-1. These are the four of the deeper site boreholes and are spread over a large area of the site. KFI04 is in the southern rock block while the others are in the northern rock block. Compared to Case 1 this variant calibrates better. The salinity below Zone 2 in the northern rock block is still a bit deep and the observed sharp transition is only reproduced partially, as can be seen for BFI01 and KFI06. This indicates that the positioning and properties of Zone 2 may needs more fine-tuning to get a more precise match.

Figure 5-16 - Figure 5-18 present the exit locations for the 120 released particles in the variable density simulation and the freshwater simulation of Case 3. Again, the exit locations are limited to Zone 5 and the Imundbo Zone and do not differ much from the other variants.
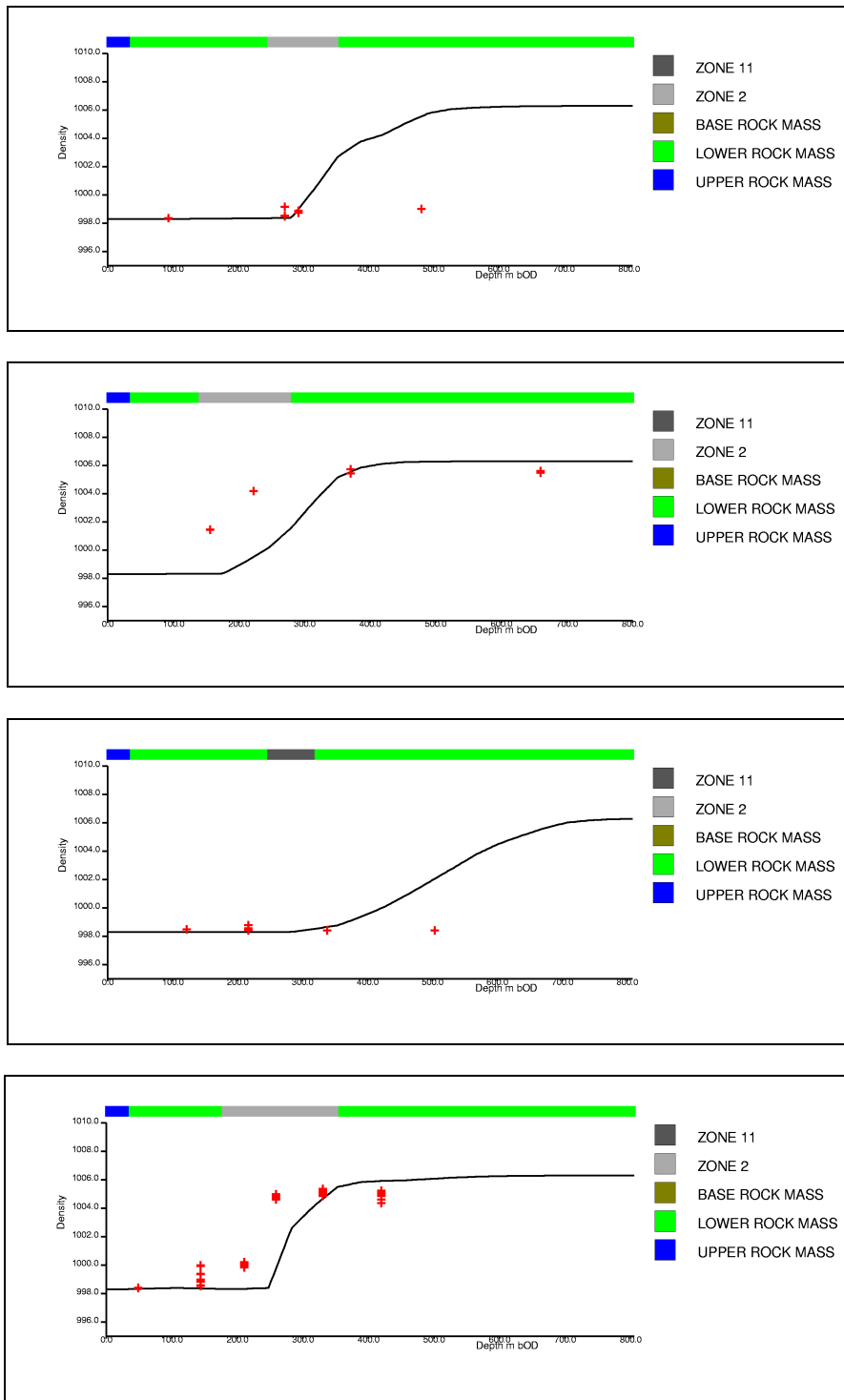
Figure 5-15   Salinity in the boreholes BFI01, KFI04, KFI06 and KFI07 (from bottom to top) for Case 3, see Figure 5-1. The solid lines represent the model results. The red crosses are experimental data. The depth of the model is shown on the x-axis with the top to the left. The range of density shown on vertical axis is 996 to 1010 kgm^{-3}.
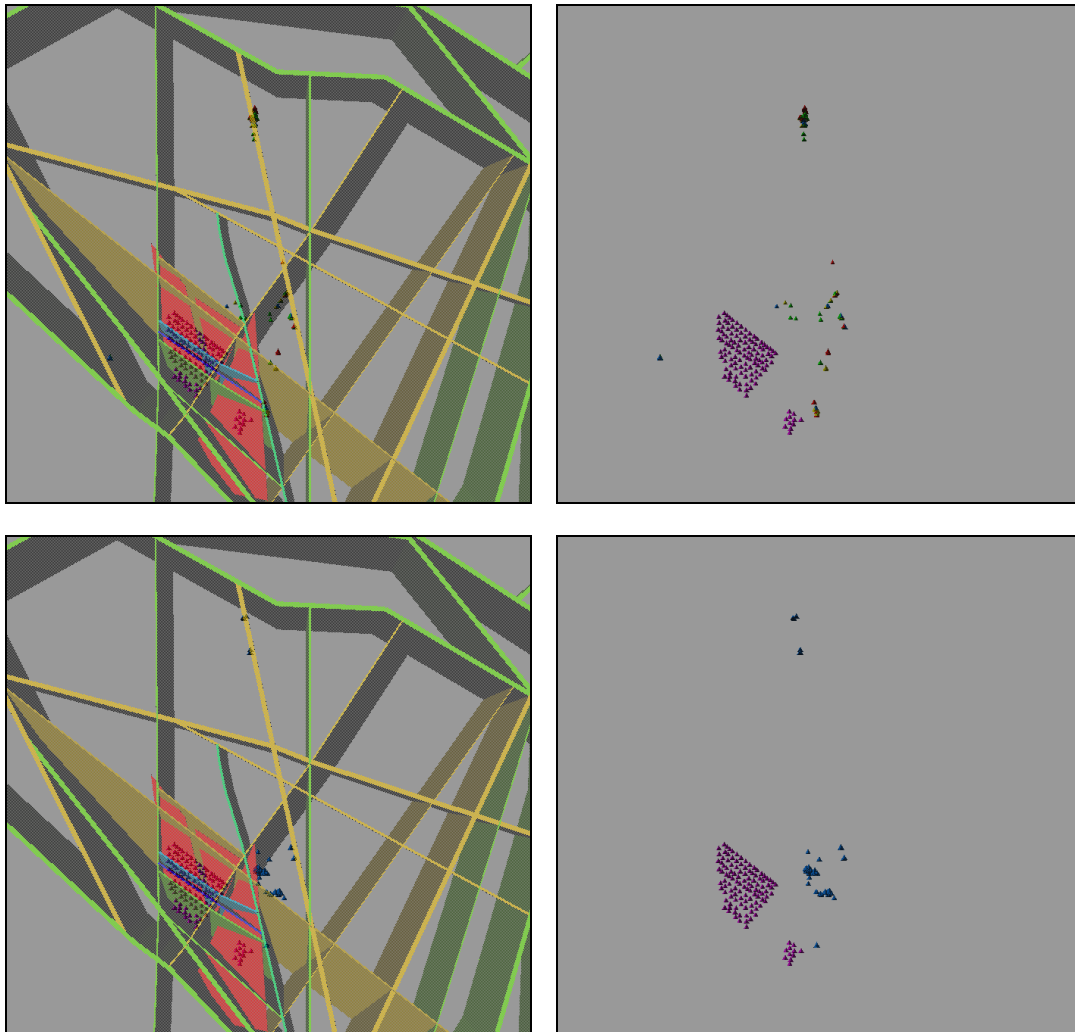
Figure 5-16   *Exit locations (blue-green markers) for Case 3 shown together with the starting positions (purple markers). Fracture zones removed for clarity in the pictures on the right side. Top: Variable density simulation. Bottom: Freshwater simulation.*

Figure 5-19 presents a close up view from above of the iso surfaces of the salt concentration at $c = 0.25$ (left column) and $c = 0.75$ (right column) together with fracture zones. The iso surfaces are shown at three different times: 3000 BP (top), present time (middle) and 5000 AP (bottom). It is clear that freshwater has replaced the saline water in the fracture zones very early in the simulation. The salinity in the rock blocks is relatively high but it decreases as the time increases.

Figure 5-20 presents Zone 2 (red) superimposed on a slice coloured with respect to the salt concentration. The slice is cutting through the model in a north-south direction and is viewed from the east. The offset between the two parts of Zone 2 appears clearly and so does the sharp transition of salinity across Zone 2. The higher salt concentration follows Zone 2 on the bottom side. The dips in salinity present in the picture arise from fractures that have been removed for visibility.
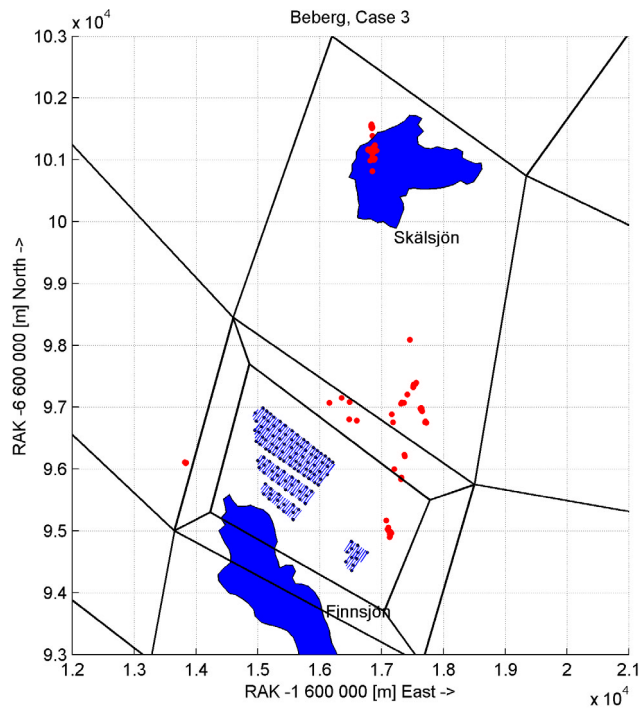
Figure 5-17 *Exit locations (red markers) for Case 3 (variable density simulation) shown together with the starting positions (black markers). The patch grid and some surface features have been included for orientation.*
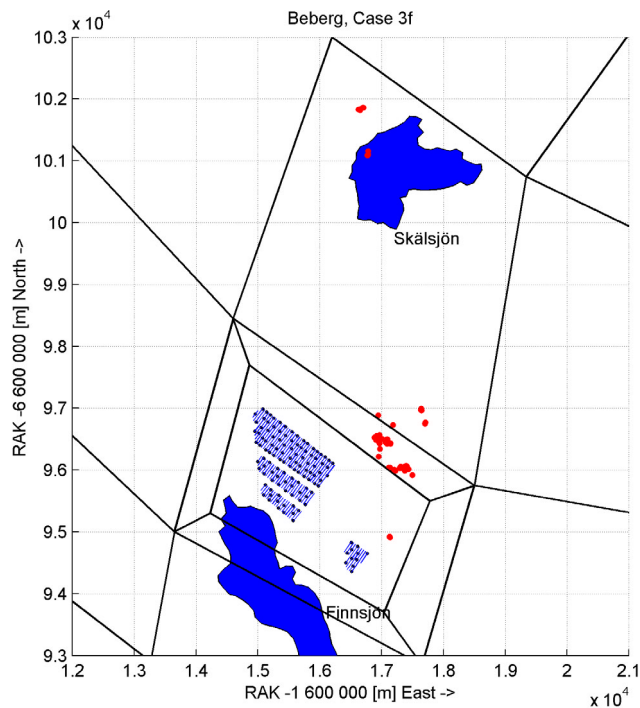
Figure 5-18 *Exit locations (red markers) for Case 3f (freshwater simulation) shown together with the starting positions (black markers). The patch grid and some surface features have been included for orientation.*
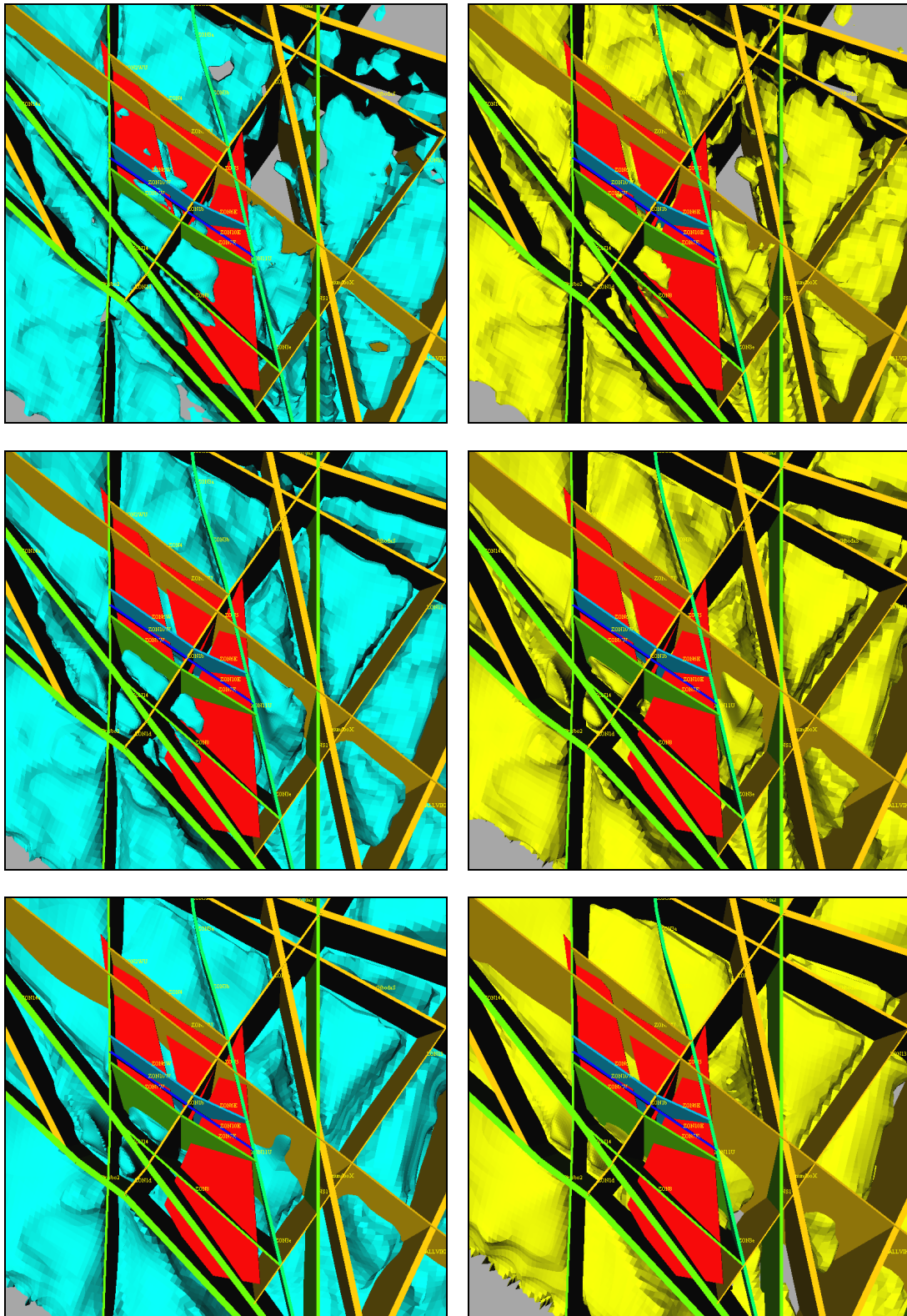
*Figure 5-19   Iso surfaces of the salt concentration at c = 0.25 (left column) and
c = 0.75 (right column) shown together with fracture zones. Top: 3000
BP; Middle: Present time; Bottom: 5000 AP. Close up view from
above the repository area. View from above.*
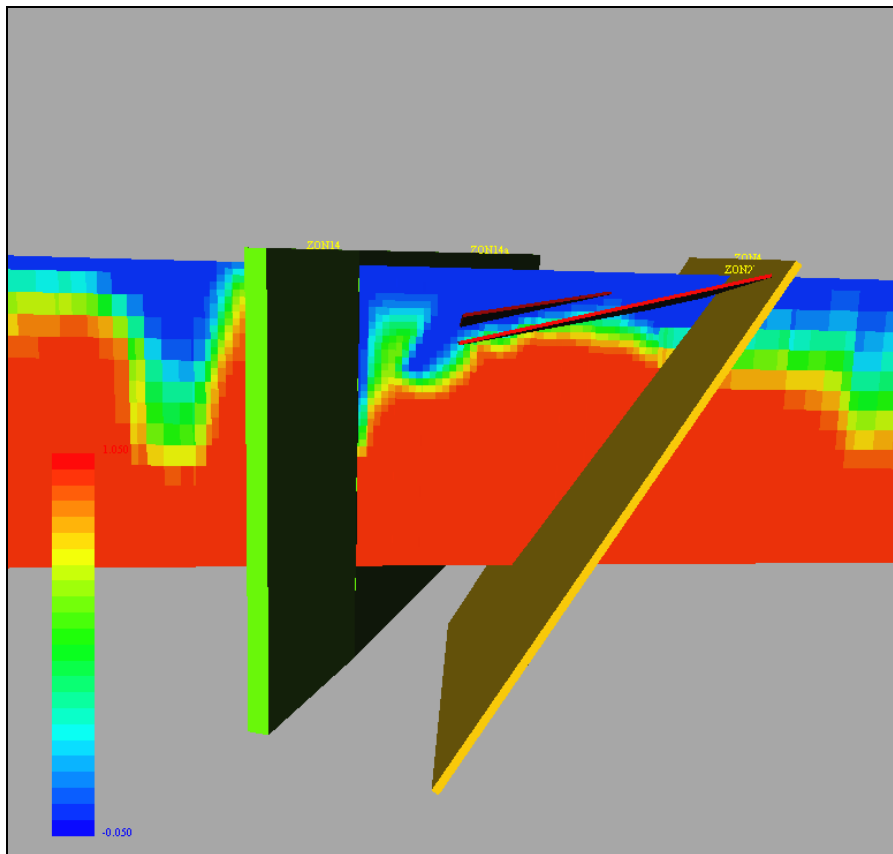
Figure 5-20   *Zone 2 (red) superimposed on a slice coloured with respect to the salt concentration. The blue colour is indicating low salinity and red is indicating high salinity. The slice is cutting through the model in a north-south direction and is viewed from the east. Zone 5 (yellow) and Zone 14 (green).*

In Table 5-3 a statistical summary for 120 starting positions for Case 3 is presented. In the summary, statistics for particles released at four different times in the variable density simulation is presented together with the results for the freshwater simulation. The travel times and the path lengths have increased somewhat compared to Case 1. The difference in log-scale might seem small but the travel time has increased about 20% in Case 3 compared to Case 1 while the path length has increased more than 30%. The reason is that most particles are now starting in or below the saline transition zone which will tend to cause particles to initially move downwards at least until they reach a fracture zone, and hence have longer paths. The difference made by releasing the particles at different times is not as obvious as in Case 1. Here, the change in the performance measures is only marginal.

	Present time	1000 yrs	3000 yrs	4750 yrs	Freshwater
Log$_{10}$(TT *[yrs]***)**					
Median	2.515	2.511	2.480	2.497	2.428
5th Percentile	2.085	2.077	1.277	1.824	1.937
25th Percentile	2.336	2.330	2.259	2.264	2.294
75th Percentile	2.650	2.649	2.608	2.613	2.527
95th Percentile	2.835	2.781	2.721	2.696	2.739
Variance	0.073	0.047	0.171	0.137	0.128
Fraction	0.958	0.933	0.675	0.808	1.000
Log$_{10}$(CF *[m/yr]***)**					
Median	-3.170	-3.166	-3.174	-3.186	-3.298
5th Percentile	-3.369	-3.387	-3.358	-3.350	-3.471
25th Percentile	-3.261	-3.252	-3.255	-3.250	-3.379
75th Percentile	-3.101	-3.107	-3.126	-3.132	-3.189
95th Percentile	-2.891	-2.898	-2.895	-2.893	-2.877
Variance	0.021	0.018	0.017	0.016	0.029
Log$_{10}$(PL *[m]***)**					
Median	3.854	3.888	3.861	3.865	3.508
5th Percentile	3.596	3.604	3.062	3.383	3.339
25th Percentile	3.829	3.842	3.837	3.844	3.454
75th Percentile	3.878	3.944	3.882	3.888	3.646
95th Percentile	3.903	4.010	3.906	3.914	4.260
Variance	0.013	0.012	0.055	0.036	0.085
Fraction	0.958	0.933	0.675	0.808	1.000

Table 5-3   Statistical summary for 120 starting positions for Case 3.

5.4 Case 4

Case 4 is a stochastic simulation of 5 realisations based on the model in Case 3. The exit locations are again limited to the Imundbo Zone and the discharge areas to the north-east of the repository, see Figure 5-21 and Figure 5-22. Compared to the deterministic variants the spread in exit locations is larger. This is also confirmed by the higher variance of the performance measures, see Table 5-4. Compared to Case 3, the travel times and the canister flux are marginally lower.
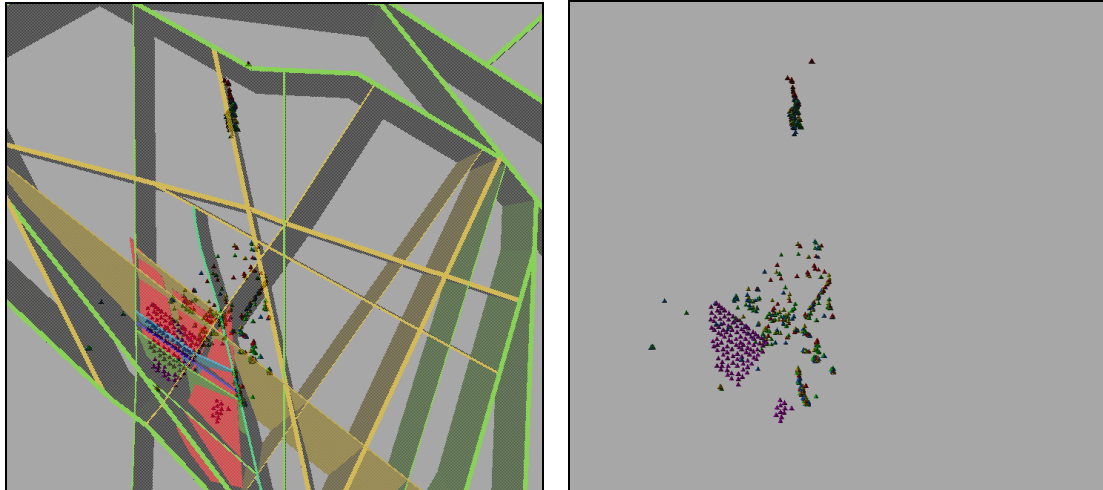
Figure 5-21   Exit locations (blue-green markers) for the stochastic simulation (5 realisations) of Case 4 shown together with the starting positions (purple markers). Fracture zones removed for clarity in the right picture.
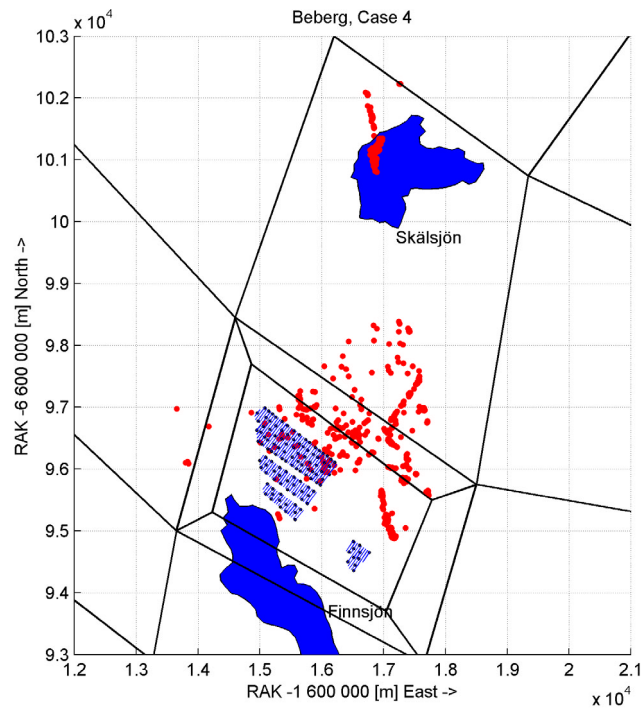
Figure 5-22   Exit locations (red markers) for Case 4 (stochastic variable density simulation with 5 realisations) shown together with the starting positions (black markers). The patch grid and some surface features have been included for orientation.

	Present time	1000 yrs	3000 yrs	4750 yrs
$Log_{10}(TT$ *[yrs]*$)$				
Median	2.492	2.480	2.380	2.393
5th Percentile	1.243	0.991	0.957	0.857
25th Percentile	2.218	2.140	2.146	2.160
75th Percentile	2.758	2.663	2.549	2.566
95th Percentile	3.077	3.041	2.791	2.928
Variance	0.288	0.343	0.264	0.346
Fraction	0.743	0.593	0.703	0.622
$Log_{10}(CF$ *[m/yr]*$)$				
Median	-3.248	-3.232	-3.231	-3.237
5th Percentile	-4.253	-4.210	-4.181	-4.153
25th Percentile	-3.690	-3.670	-3.651	-3.654
75th Percentile	-2.879	-2.892	-2.879	-2.886
95th Percentile	-2.335	-2.301	-2.279	-2.297
Variance	0.367	0.357	0.351	0.350
$Log_{10}(PL$ *[m]*$)$				
Median	3.867	3.866	3.866	3.873
5th Percentile	3.159	3.076	3.087	3.035
25th Percentile	3.828	3.830	3.834	3.836
75th Percentile	3.915	3.909	3.893	3.902
95th Percentile	4.367	4.018	3.923	3.937
Variance	0.096	0.075	0.063	0.088
Fraction	0.743	0.593	0.703	0.622

Table 5-4   *Statistical summary for 5 realisations of 120 starting positions for Case 4.*

5.5 Case 5

Case 5 is a variant based on Case 3 with the difference that the zones surrounding and intersecting Zone 2 and Zone 11 were truncated more exactly, i.e. in the same way as was used in Case 2. Thus, in Case 5 Zone 2 is represented as in Andersson et al. (1991) where it was interpreted as two parts (east and west).

The results are not much different from Case 3 so the more exact truncation of zones does not seem to have any significant effect on the results. Figure 5-23 shows the predicted salinity profiles in the deep boreholes along with the measured values. Profiles are shown for the boreholes BFI01, KFI04, KFI06 and KFI07, see Figure 5-1. These are the four of the deeper site boreholes and are spread over a large area of the site. KFI04 is in the southern rock block while the others are in the northern rock block. The salinity profiles are nearly identical to Case 3 which means that the salinity below Zone 2 in the northern rock block is still a bit deep and the observed sharp transition is only reproduced partially, as can be seen for BFI01 and KFI06. In order to get a better calibration more effort has to be put into the positioning and the properties of Zone 2.

Figure 5-24 presents the exit locations for the 120 released particles in Case 5. The exit locations are similar to Case 3.

In Table 5-5 a statistical summary for 120 starting positions for Case 5 is presented. In the summary, statistics for particles released at four different times in the variable density simulation is presented together with the results for the freshwater simulation. The performance measures are essentially the same as for Case 3.
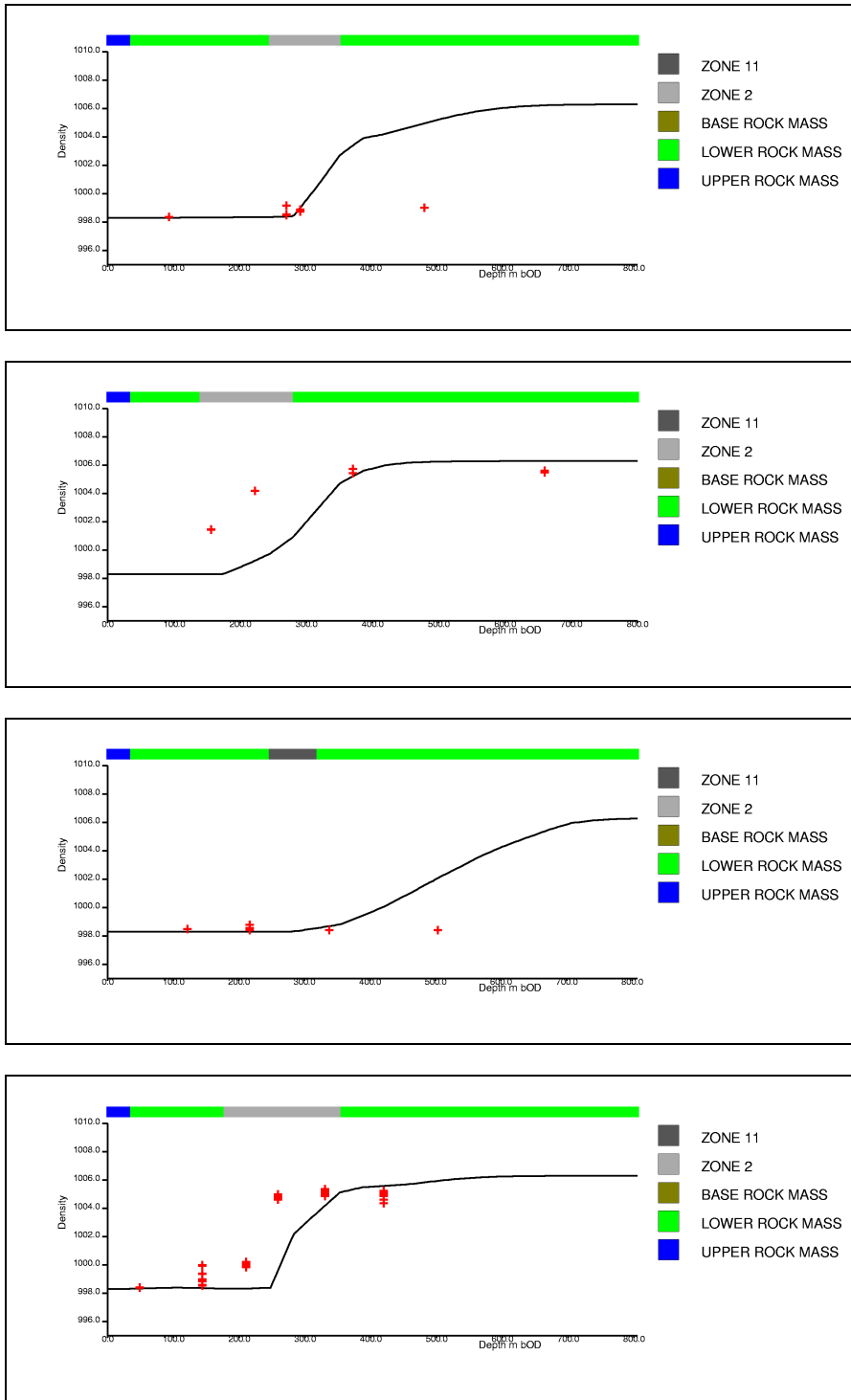
Figure 5-23   Salinity in the boreholes BFI01, KFI04, KFI06 and KFI07 (from bottom to top) for Case 5, see Figure 5-1. The solid lines represent the model results. The red crosses are experimental data. The depth of the model is shown on the x-axis with the top to the left. The range of density shown on vertical axis is 996 to 1010 kgm^{-3}.
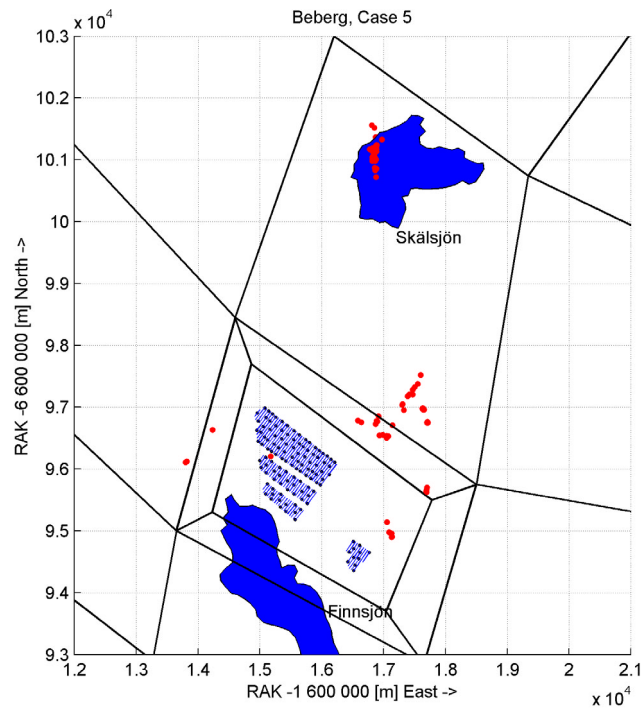
Figure 5-24   Exit locations (red markers) for Case 5 (variable density simulation)
shown together with the starting positions (black markers). The patch
grid and some surface features have been included for orientation.

	Present time	1000 yrs	3000 yrs	4750 yrs
Log$_{10}$(TT *[yrs]*)				
Median	2.448	2.452	2.467	2.476
5th Percentile	1.803	1.868	1.884	1.917
25th Percentile	2.271	2.271	2.275	2.284
75th Percentile	2.585	2.597	2.591	2.589
95th Percentile	2.686	2.704	2.673	2.689
Variance	0.099	0.095	0.083	0.111
Fraction	0.967	0.942	0.892	0.975
Log$_{10}$(CF *[m/yr]*)				
Median	-3.138	-3.137	-3.141	-3.148
5th Percentile	-3.335	-3.329	-3.325	-3.297
25th Percentile	-3.256	-3.253	-3.227	-3.210
75th Percentile	-3.056	-3.068	-3.084	-3.090
95th Percentile	-2.920	-2.938	-2.946	-2.942
Variance	0.017	0.015	0.012	0.011
Log$_{10}$(PL *[m]*)				
Median	3.851	3.869	3.862	3.868
5th Percentile	3.609	3.609	3.640	3.615
25th Percentile	3.828	3.838	3.841	3.851
75th Percentile	3.872	3.916	3.882	3.890
95th Percentile	3.904	4.055	3.911	3.916
Variance	0.019	0.030	0.020	0.038
Fraction	0.967	0.942	0.892	0.975

Table 5-5   Statistical summary for 120 starting positions for Case 5.

5.6 Comparison with SR 97

Table 5-6 presents a comparison between the two deterministic freshwater variants (Case 1f and Case 3f) in the present study and previous studies (deterministic as well as stochastic) for SKB covering the Beberg site. Generally, the present study shows longer travel times and lower canister fluxes compared to previous studies even if the differences in the performance measures are not very large. Some of the discrepancies can be explained by the different structural models used. In the HYDRASTAR model of SR 97, a higher conductivity in the repository rock block was used which gave shorter travel times compared to the NAMMU models. There is, however, more consistency between the current models and the recent stochastic NAMMU model (Marsic *et al*., 2001) where the hydraulic conductivity in the repository block was not modified. An interesting effect of the more complex structural model used in Case 3 is that the variance of travel time and canister flux are reduced. This is because the semi-impermeable core of Zone 2 and the truncation of vertical zones against the top of Zone 2 has removed a few fast paths. Another important result is that travel times for Case 3 are the longest, and this is the case with the best match to salinity measurements. This shows the importance of modelling the structural interpretation of fracture zones accurately.

Table 5-7 presents a comparison between the two deterministic variable density variants (Case 1 and Case 3) in the present study and previous studies (deterministic as well as stochastic) at SKB covering the Beberg site. The results for the travel time in Cases 1 and 3 are of similar magnitude to the regional NAMMU model of SR 97. The results are also compared to the SR 97 HYDRASTAR model for the case where the boundary conditions used were taken from the environmental head calculated in the saline regional model. That case did not explicitly include salt in the model, so the groundwater flow conditions at repository depth were different to those in the current study. The results from Marsic and Hartley (2000) were based on the SR 97 hydraulic conductivity model, but with salinity represented explicitly. This gave slightly longer travel times compared to SR 97, showing that salinity was giving longer travel times due to longer pathlines. Here, the saline variants again result in longer travel times and path lengths compared to the freshwater simulation. Again, the main reason for the differences compared to the SR 97 HYDRASTAR model is the enhanced hydraulic conductivity in the repository block used for SR 97.

	Case 1 freshwater(D)	Case 3 freshwater(D)	BaseFine Case R-00-14 (D)	NAMMU R-01-49 (S)	Variant 4 SR 97 (D) TR-99-18	Base Case SR 97 (S) TR-99-18
Log$_{10}$(TT *[yrs]***)**						
Median	2.041 (110)	2.428 (268)	1.828 (67)	2.308 (203)	1.433 (27)	1.755 (57)
25th Percentile	1.576	2.294	1.510	1.790	1.230	1.462
75th Percentile	2.418	2.527	1.958	2.727	1.631	2.023
Variance	0.358	0.128	0.206	0.691	0.108	0.237
Log$_{10}$(CF *[m/yr]***)**						
Median	-3.520	-3.298	-2.706	-3.418	-2.732	-2.923
25th Percentile	-3.835	-3.379	-2.837	-4.014	-2.817	-3.322
75th Percentile	-3.174	-3.189	-2.503	-2.829	-2.529	-2.519
Variance	0.483	0.029	0.136	1.108	0.162	0.423
Log$_{10}$(PL *[m]***)**						
Median	3.533 (3412)	3.508 (3221)	-	3.524 (3342)	-	-
25th Percentile	3.437 (2735)	3.454 (2844)	-	3.433 (2710)	-	-
75th Percentile	3.578 (3784)	3.646 (4426)	-	3.589 (3882)	-	-
Variance	0.018	0.085	-	0.018	-	-

Table 5-6   *Comparison between the freshwater simulations in Case 1 and Case 3 and previous studies at SKB covering the Beberg site. (D) is used to indicate a deterministic case with statistics taken over 120 start positions, (S) a stochastic case with ensemble averaging over realisations and start positions. A uniform transport porosity of 10^{-4} was used calculating the transport statistics within all compared studies listed above.*

	Case 1 saline (D)	Case 3 saline (D)	Saline Case R-00-14 (D)	Variant 1 SR 97 (S) TR-99-18	SR 97 saline regional (D) TR-98-24 [*]
$Log_{10}(TT$ _[yrs]_$)$					
Median	2.443 (277)	2.515 (327)	1.709 (51)	1.544 (35)	2.450 (282)
25th Percentile	1.627	2.336	1.686	1.279	-
75th Percentile	2.589	2.650	1.714	1.794	-
Variance	0.544	0.073	0.003	0.259	-
$Log_{10}(CF$ _[m/yr]_$)$					
Median	-3.099	-3.170	-2.424	-2.588	-
25th Percentile	-3.301	-3.261	-2.506	-2.963	-
75th Percentile	-2.919	-3.101	-2.346	-2.198	-
Variance	0.335	0.021	0.028	0.474	-
$Log_{10}(PL$ _[m]_$)$					
Median	3.731 (5383)	3.854 (7144)	-	-	-
25th Percentile	3.494 (3119)	3.829 (6745)	-	-	-
75th Percentile	3.799 (6295)	3.878 (7551)	-	-	-
Variance	0.039	0.013	-	-	-

Table 5-7   *Comparison between the variable density simulations in Case 1 and Case 3 and previous studies at SKB covering the Beberg site. (D) is used to indicate a deterministic case with statistics taken over 120 start positions, (S) a stochastic case with ensemble averaging over realisations and start positions. A uniform transport porosity of 10^{-4} was used calculating the transport statistics within all compared studies listed above. [*] In the regional model of SR 97, only 16 starting positions were used for the pathline calculations.*

6 Summary and future work

This section summarises developments to the methodology and software required to perform this project, the results and findings of the modelling, and recommendations for further work and developments

6.1 Development summary

Detailed descriptions of some of the developments to the methodology are given in Sections 2 and 3. Here, is a summary of these and other developments to NAMMU and Avizier for NAMMU that were required to complete this task.

1) **Boundary conditions:** more efficient implementation of hydrostatic boundary condition for pressure with variable density groundwater. New non-linear boundary condition definition implemented for salinity on the top and vertical surfaces. Recent time-varying boundary condition facility (as of NAMMU 7.0) used to describe post-glacial rebound. These developments were required for an efficient and flexible representation of the evolving physical conditions.

2) **Solver method for transient salt:** solution of flow and salt transport equations de-coupled into a two-step process at each time-step based on a linearisation of the equations. This gives a stable and efficient scheme providing the above boundary conditions were used.

3) **Efficiency of solver:** the size of the internal element data file has been further reduced by only storing the Gauss point weights and positions and recalculating the basis functions and their derivatives as they are used. This represents an incremental improvement on solver times and disk requirements.

4) **Modelling rock blocks/volumes:** a new facility to change the rock type and properties of finite-elements within a defined block has been implemented. This allows the representation of rock volumes that are non-planar, and is fully integrated with IFZ. For example, rock blocks such as the 'Northern rock block' and 'Southern rock block' could be represented. In this study the wedge shaped Zone 2 was modelled using this facility. It allows either the rock type or permeability to be changed within a volume delimited by several planes. It is also possible to modify the statistical properties of a block for stochastic continuum models. The only limitation is that if a fracture zone is modelled in this way it has a lower priority than one modelled using IFZ. For example, if a low permeability zone is modelled as a rock block and it intersects a high permeability zone represented by IFZ, then the high permeability zone will dominate at the intersection, and there is no way currently that the user can assign priority to the low permeability zone. Further work is required to offer greater flexibility.

5) **Fracture zone porosity:** IFZ has been extended to calculate an effective porosity in addition to the permeability. This is calculated on an element-by-element basis as a volume-weighted average of the total porosities of fractures and rock mass. Additional options may be required in the future such as calculating fracture porosity only as an appropriate porosity for advective transport.

6) **Avizier for NAMMU:** improvements to the fracture zone Dialog to allow individual fractures to be selected. Display of objects (used to show particle start and exit locations, and salinity values, for example) as tetrahedral volumes to improve efficiency and support viewing many thousands of objects. Support viewing of transient solutions (ongoing).

6.2   Conclusions

The main focus of this project was to develop and test a methodology for performing large simulations of transient variable density flow. Therefore, the following lists a set of generic conclusions as well as ones more specific to the test study of the Beberg site:

1) **Feasibility:** it is numerically feasible to construct large (0.5 million elements) embedded models of transient variable density flow with a relatively fine mesh (about 35m) of the site-scale.

2) **Stochastic simulation:** performing stochastic realisations of long transients is just possible, although the requirements on CPU and disk to store the results for 100 realisations, say, would be significant. As an indication, about 19 realisations of the current model could be run on a Sun Enterprise 450 (4 × UltraSPARC-II 400MHz) computer in one week if all four processors are fully utilised.

3) **Embedded grid:** the nesting of a refined site-scale model (35m elements) within a coarser (100m) regional-scale mesh for variable density flow was tested successfully. It was found that grading the refinement around the site-scale to avoid a large step change in element size was beneficial for convergence and stability. This may be less of an issue if a more sophisticated preconditioner was used.

4) **Solver:** the most efficient and stable scheme was obtained by decoupling the flow and transport equation at each time-step. GMRES was the most robust conjugate gradient method for this problem.

5) **Boundary conditions:** a set of relatively complex non-linear boundary conditions had to be applied for both pressure and salinity on the top and vertical boundaries to give the system sufficient freedom to approximate realistic conditions over a large area and long times. It was important that both flow and a flux of salinity could cross each boundary, and that the direction and magnitude could evolve in time.

6) **Calibration on salinity:** model predictions of the salinity in the deep boreholes were used to calibrate the model parameters and structural representation. As for the SR 97 regional-scale model the high salinity below Zone 2 could not be reproduced with a highly transmissive zone. A reasonable match could only be achieved if a semi-impermeable band be included in the core of Zone 2, and the position of Zone 2 had to be taken from the detailed geometry defined in Andersson *et al.* (1991) rather than SR 97.

7) **Structural model**: the calibration demonstrated the important effect that sub-horizontal fracture zones could have on deep groundwater flows, and the importance of having a good structural interpretation of such zones. Aspects such as hydraulic anisotropy, layering, fracture zone truncation and interconnection will be important to characterise in any site either by direct measurement and/or by using modelling to

test the ability of different structural models to predict hydraulic and chemical properties in deep boreholes. In fact, this is a good example of how a flow model calibration exercise can augment structural interpretation and help constrain it.

8) **Flexible representation:** new tools for representing fracture zones and rock volumes allow flexibility in how a structural model is represented e.g. wedge shaped zones and hydraulic anisotropy.

9) **Modelling barriers:** it proved to be non-trivial to model barriers since approximating the thickness or representation of flow through a thin barrier relative to the grid size can lead to an over-prediction of flow rates through barriers. For standard elements, if only a thin band of elements, one or two thick, is used to model a semi-impermeable barrier, then the flow across the zone may be larger than expected. This is because small flows can 'leak' across element corners because of the lack of localised mass balance. This is not the case with mixed-elements, which motivates more investigation of this element type.

10) **Transport statistics:** the transport statistics indicate that neither salinity nor release-time has a great effect on statistics of travel times or canister flux. Salinity leads to slightly higher canister flux, but slightly longer travel times and around double the path lengths. Perhaps more important is the structural model for Zone 2. A low permeability core in Zone 2 leads to slightly longer median travel time, but also much less variance with fewer short paths. These conclusions are very site specific. The Beberg site is located about 15km inland, and hence conclusions on the importance of release time are likely to be different to those for a site nearer the coast.

11) **Comparison with previous studies:** many of the conclusions from the SR 97 regional model have been shown to be valid for this more detailed study. For example, the same parameters and structural model were needed to get a calibration on deep salinity profiles. Travel times and exit locations are broadly consistent, and the problem with particles exiting the SR 97 model out of the vertical side has been solved by extending the model northwards. The new model shows that the exit location for these paths to be Skälsjön. Comparing with the site-scale models of SR 97 travel times are much longer here mainly because of not enhancing the permeability of the rock blocks, but also due to salinity and the structural model for Zone 2. Results are most similar to the SR 97 regional model.

6.3   Further work/recommendations

1) **RVS interface:** this task is an outstanding both in interfacing NAMMU to RVS and Avizier to RVS.

2) **Development of statistical tools for transients and path length:** better statistical tools need to be developed to handle large number of canister locations/realisations and with more flexibility for different release times as well as realisations. Other properties could be included such as path length.

3) **Structural model development and calibration:** need to ensure the site-investigation and database tools allow different structural models to be defined, tested and recorded. Need to scope different structural models of sub-horizontal zones, and have models linked to site-investigation to focus geological characterisation and conditioning/constraining of models.

4) **Near-surface modelling:** the models should be calibrated to recharge/discharge rates at the surface as a demonstration of consistency with surface hydrology data. This is likely to involve the use of mixed Dirichlet-flux boundary conditions of the sort used on modelling Ceberg in SR 97. There is also the potential to use data on the chemistry/salinity of discharged groundwater as a further control on model validation.

5) **Development of more robust iterative solvers and 3D mixed-elements:** a more robust iterative solver would improve the flexibility to model systems with a large degree heterogeneity and/or with embedded grid nesting. The problem is that heterogeneity creates ill-conditioned matrix systems, while embedded grids create large bandwidths. Hence, robust predicitioners are required. There are many such methods out in the open literature that could be tried on a few test problems developed on recent studies to benchmark robustness and speed/number of iterations. Another issue is developing iterative solvers for the mixed element option in NAMMU. The use of the mixed element formulation of finite-elements would have significant benefits over the standard formulation. This is because mixed elements solve for an explicit flux variable to give local as well as global mass balance. In consequence, the method offers better accuracy where there are large contrasts in permeability over the scale of a few elements e.g. around fracture zones, and particular thin barriers; it also gives a continuous velocity field that will make pathline calculations more robust. Some work in this area has been performed in collaboration with the University of Bath, UK.

6) **Implementation of solution schemes for salt transport:** the decoupled numerical scheme detailed in Section 3 provided an efficient solution method for the non-linear transient transport equations. However, the method was set up to order the solves: first obtain a pressure solution consistent with the salinity distribution at the previous timestep; and then update the salinity based on the velocity field based on this new pressure distribution. The problem with this is that when calculating pathlines NAMMU will calculate a flow field based on the pressure and salinity distributions from the same timestep, but these will not be consistent. Essentially, the correct approach would be to take the salinity from the required timestep and the pressure from the next timestep. This problem could be solved by swapping the

order in which pressure and salinity are calculated, although something special may have to be done to ensure pressure and salinity are consistent for the first timestep (i.e. the initial condition). This would be an easy change to make and would likely improve accuracy in the pathline calculation, especially if large timesteps are used.

7) **Development of more robust pathline methods:** the algorithm used to calculate pathlines through heterogeneous models with complex structures, thin features with high permeability contrasts, and in particular barriers needs to be very robust. Some recent work following on from this project has developed a more robust method in NAMMU/CONNECTFLOW for tracking particles through a heterogeneous medium. The main change was to choose the timestep for each step along the path based on the advective velocity field in the local coordinate system. This is to ensure that the paths track accurately across each element without stepping over any thin elements or ones with high permeability contrasts. There is still a potential problem with the standard element formulation that due to the lack of local mass balance, then particles can become stuck. The new implementation of particle tracking detects when this happens and moves the particle on with a mean local velocity for elements in proximity to the problem area. Although the results reported here were based on the old pathline algorithm, it was verified that the new algorithm worked for these models and that fewer particles became stuck, especially at the later start times.

7   References

Andersson J-E, R. Nordqvist, G. Nyberg, J. Smellie and S. Tiren, 1991, *Hydrogeological conditions in the Finnsjön area. Compilation of data and conceptual model*, SKB TR 91-24.

Cliffe K. A., S.T. Morris and J.D. Porter, 1998*, Assessment Model Validity Document; NAMMU: A program for calculating groundwater flow and transport through porous media,* SKB R-99-51.

Gylling B., D. Walker and L. Hartley, 1999, *Site-scale groundwater flow modelling of Beberg,* SKB TR-99-18.

Hartley L., A. Boghammar, B. Grundfelt, 1998*, Investigation of the large scale regional hydrogeological situation at Beberg***,** SKB TR-98-24.

Marsic N., and L. Hartley, 2000, *Modelling of the Site Scale Hydrogeological situation at Beberg Using NAMMU,* SKB R-00-14.

Marsic N., L. Hartley, C.P. Jackson and M. Poole, 2001, *Development of Hydrogeological Modelling Tools Based on NAMMU,* SKB R-01-49.